Version 1.1: June 20, 1996

Version 1.0: June 7, 1996

STAR Note 247

TPC: Algorithms, Gain and R-ϕ Resolution with P10

R. Bossingham
Nuclear Science Division
Lawrence Berkeley National Laboratory

Previous discussions of the TPC r-ϕ resolution and of noise effects with P10 are extended to consider ionization statistics and alternatives to the three-pad hit-reconstruction algorithm. Estimates of the required gas gain and obtainable resolution are given; these are relevant to the TPC calibration, tracking and simulation efforts.

Introduction

The TPC gas gain and hit-reconstruction algorithm are needed for realistic studies of calibrations, or of physics involving stiff tracks, kinks, etc. Of course, momentum resolution for a typical track in the STAR TPC with a P10 filling is limited by multiple scattering, not individual hit resolution, so not all results are sensitive to fine tuning. The basic goals in this note are to:

- Calculate an absolute TPC gas gain, above which there is little further improvement in physics data; achieving the base resolution from the STAR Conceptual Design Report is a reasonable choice.
- Compare simple hit-reconstruction algorithms, finding ranges of applicability and resolution. The intent is not to determine the most accurate algorithm—presumably a maximum-likelihood fit—but to find a good one that is acceptably fast.

Gain and Pad Response in the STAR TPC

The definitions of "gain" and "pad response" for the STAR TPC need some explanation. The anode wire current is expected[1] to develop with time as $I(t) = I_0/(1 + t/t_0)$ initially; t_0 is of

[1] F. Sauli, CERN 77-09 (1977).

order 1 ns. (Sauli derives this for a cylindrical proportional chamber and constant ion mobility.) Integrating, $Q(t_{\max}) = I_0\, t_0 \ln(1 + t_{\max}/t_0)$, where $t_{\max}$ is typically some tens of microseconds.

Consider a STAR inner TPC subsector ("2-2 mm" design, without field wires), assuming P10 gas and 1100-V anode potential; $t_0 = 1.5$ ns and $t_{\max} = 62$ μs. The first 45% of the charge is collected within 180 ns, but the next 45% requires 22,000 ns. In practice, anode signals are usually AC-coupled and thereby differentiated to some extent; even DC-coupled signals are often distorted by leakage currents on these time scales.

Practical detectors seldom integrate the total charge, and the STAR TPC is no exception. The FEE electronics have a 180-ns shaping time (FWHM) and include tail-cancelation circuitry, so the collected charge represents 45% of the total. On the other hand, for practical reasons, STAR gain studies use a shaping time of 308 ns (FWHM), obtained with an integrating preamp and an LBL-built 21X1011P-1 amplifier set to a 200-ns "peaking time." These gain measurements must be scaled to be applied to STAR; extrapolating existing measurements of signal versus shaping time,[2] the factor is ~0.90 for an outer TPC subsector at 1200V. In this case, $t_0 \approx 1.8$ ns, so

$$\frac{Q(180\ \mathrm{ns})}{Q(308\ \mathrm{ns})} = \frac{\ln\left[1 + (180\ \mathrm{ns})/t_0\right]}{\ln\left[1 + (308\ \mathrm{ns})/t_0\right]} = 0.90\ .$$

Although t_0 is not a constant, the scale factor is within the 0.89–0.90 range for either subsector at reasonable voltages. Gains in this note are those for the 180-ns shaping time.

There is another potential complication affecting the pad signal—avalanches do not, in general, uniformly surround the anode wire, so the signal-developing ions do not drift away from the wire isotropically. This is seen in simulations.[3] A given signal electron drifts to an anode wire through one of four channels between the ground wires, resulting in avalanches which are preferentially on the anode wire surface opposite the pad plane. The ions, then, tend to drift away from the pad plane, and the pad signal current reverses sign after $\sim 11\mu$s,[4] presumably because of this. This is consistent with a ratio of 2:1 for ions drifting away:toward the pad plane.

After the ion centroid shifts away from the anode wire, the pad response function varies with time in a way that depends upon the distribution of the avalanche around the wire (and, therefore, gain). This should not occur within the FEE shaping time, although the accuracy of the FEE tail cancelation could be affected.

---

[2] Draft STAR Note, W. Betts *et al.*

[3] M. Matoba et al., *IEEE Trans. Nucl. Sci.* **NS-32**, 541 (1985).

[4] H. Wieman.

Three-Pad Algorithm

The TPC Clusterfinder[5] uses the PEP4 three-pad algorithm[6] by default. This algorithm was also used to estimate the STAR TPC resolution[7] and allowable noise:signal ratio.[8] The algorithm relies upon the fortuitous resemblance of the pad response function to a Gaussian. The surface charge d^2q/dA induced on a pad of width w by a linear charge density λ midway between two plates separated by D can be approximated as[9]

$$\frac{d^2q}{dA} = -\frac{\lambda}{2D}\frac{1}{\cosh(\pi x/D)} \ .$$

If, instead of an infinitely long charge distribution, one has a point charge q_0 and an infinitely long pad, the charge density across the pad is similar:

$$\frac{dq}{dx} = -\frac{q_0}{2D}\frac{1}{\cosh(\pi x/D)} \ .$$

Integrated, the pad response function is

$$P_0(x) = \int_{x_1}^{x_2} \frac{dq}{dx} = -\frac{q_0}{2\pi}\left[\arctan\left(\sinh u\right)\right]_{\pi x_1/D}^{\pi x_2/D} \ .$$

For the STAR TPC, $w/D = 0.8375$ for either subsector in the approximation that the inter-pad spacing can be ignored, so

$$P_0(0) = -\frac{q_0}{2\pi}\left[\arctan\left(\sinh u\right)\right]_{-\pi w/2D}^{\pi w/2D} = 0.333\, q_0 \ .$$

Measurements[10] gave 0.30 (inner pads) and 0.34 (outer pads). The calculated induced-charge distribution and pad response function are displayed in Fig. 1.

Real pad signals, even for tracks at zero crossing angle, represent a superposition of pad response functions due to transverse electron diffusion. Figure 2 shows the effective response functions due to diffusion; the amplitudes for zero diffusion were normalized to the measured couplings. The amplitude on the central pad is reduced: for $\sigma_{\rm dif} = 0.185$ cm and $\sigma_{\rm dif} = 0.262$ cm, it becomes 72.24% and 59.65% (inner pads) and 90.21% and 82.71% (outer pads), relative to the $\sigma_{\rm dif}$=0 case. Such diffusion widths result from 1-m and 2-m drifts along a a 0.5-T magnetic field in P10.

---

[5] STAR Note SN0238, M. A. Lisa (1996).

[6] G. Lynch, PEP4 Note TPC-LBL-78-17 (1978).

[7] STAR Note SN0034, P. G. Jones and G. Rai.

[8] STAR Note SN0137, H. Wieman and I. Sakrejda (1993).

[9] *Particle Detection with Drift Chambers*, W. Blum and L. Rolandi, published by Springer-Verlag, 1993, pp.159–162.

[10] Draft STAR Note, W. Betts *et al.*

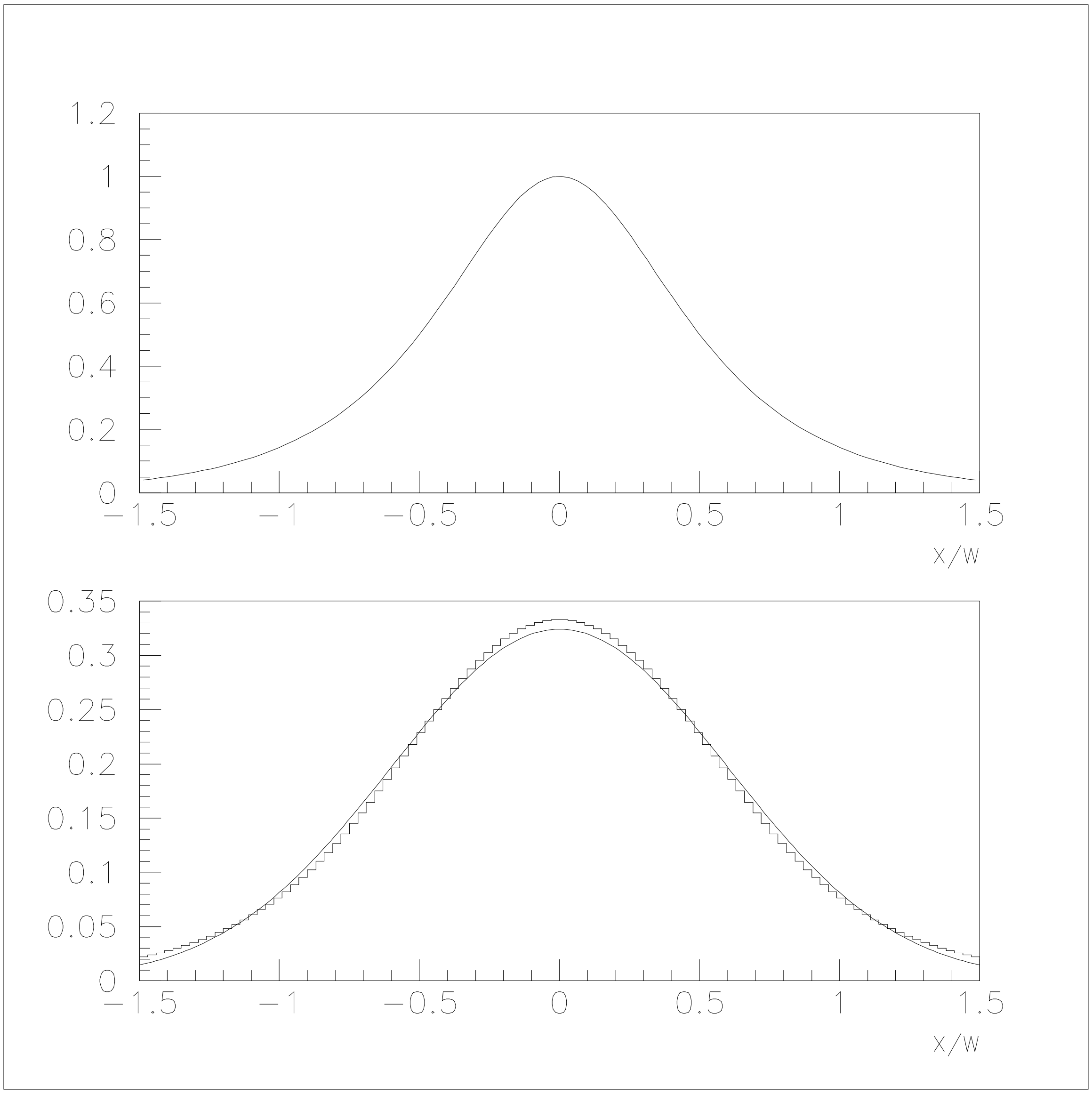

Figure 1: a) Distribution of induced pad plane charge, normalized to unity at x=0. b) Calculated pad response (histogram) for unit charge, with a Gaussian fit over the plotted range. In this approximation, inner and outer pad response functions are identical.

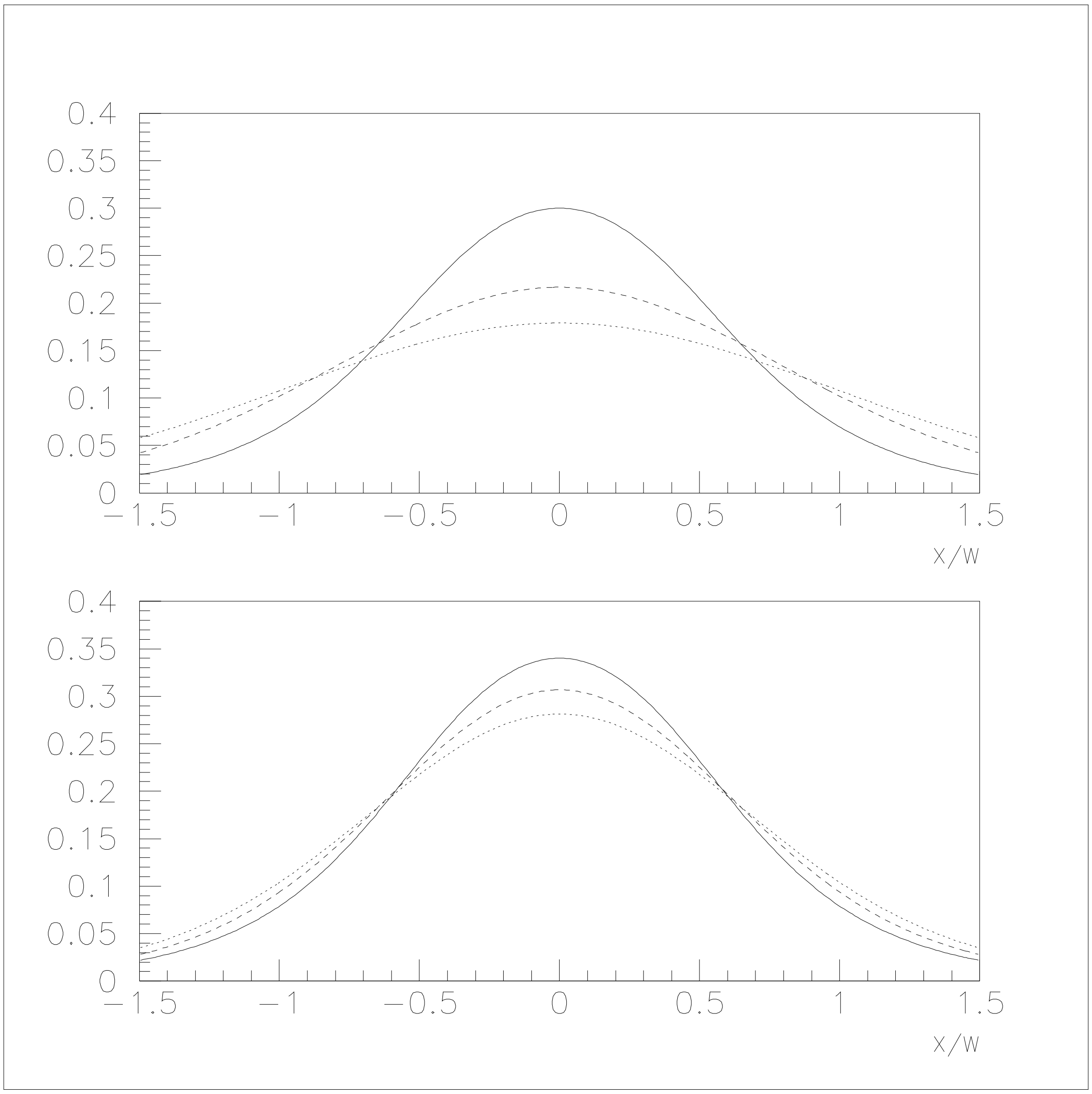

Figure 2: Calculated pad response functions per unit charge for a) inner pads and b) outer pads; curves are for diffusion widths of $\sigma_{\mathrm{dif}} = 0$ (solid line), $\sigma_{\mathrm{dif}} = 0.185$ cm (dashed line) and $\sigma_{\mathrm{dif}} = 0.262$ cm (dotted line).

Some key equations from SN0137 follow. For a track over pad 2 with zero crossing angle, displaced from the center by x, the signals on the three nearest pads are approximately

$$h_1 = h_c \exp\left[-\frac{(x+w)^2}{2\sigma^2}\right], \quad h_2 = h_c \exp\left(-\frac{x^2}{2\sigma^2}\right) \quad \text{and} \quad h_3 = h_c \exp\left[-\frac{(x-w)^2}{2\sigma^2}\right],$$

where h_c is the pad signal for a centered avalanche; σ is the pad response function width broadened by transverse diffusion; and w is the pad width and pitch. Then,

$$\sigma^2 = \frac{w^2}{\ln\left(h_2^2/h_1 h_3\right)} \quad \text{and} \quad x = \frac{\sigma^2}{2w} \ln\left(\frac{h_3}{h_1}\right).$$

The three-pad algorithm is usually applicable even if the signal on only two pads exceeded threshold—an implicit measurement still exists for the third pad. In fact, this knowledge may be almost as good as an actual measurement: if the noise is 1 count and the threshold is 3 counts above the pedestal, assuming signal of 1.5 is a good approximation.

Bias in the Three-Pad Algorithm

The Gaussian approximation in the three-pad algorithm *is* an approximation. If one evaluates h_i by integrating the induced signal and Gaussian diffusion over pad i and applies the above formulae, the derived x is biased as in Fig. 3. In the absence of noise, statistical fluctuations, etc., some $\tilde{\sigma}(x)$ gives zero bias when it replaces the fitted σ. The ratio $\tilde{\sigma}/\sigma$ is plotted in Fig. 4.

Interestingly, when $\tilde{\sigma}$ replaces the fitted σ in a realistic Monte Carlo of the TPC, resolution worsens for tracks with small-to-moderate crossing angles. Resolution for real tracks in the EOS TPC is also said to have worsened when this was done. The improvement at large crossing angles is not very useful, since other algorithms usually do at least as well there.

A solution is to scale the fitted σ's by curves like those in Fig. 4. Including the dependence on the track crossing angle α, they can be parametrized as $\tilde{\sigma}(x)/\sigma(x) = a(\alpha) + b(\alpha)(2x/w)^2$. This eliminates the bias without imposing a width in strong conflict with the fit. Strictly speaking, the correction involves iteration or the solution of a quartic equation, though this was not done for the simulations for this note. When resolution is dominated by noise rather than bias, the improvement over the uncorrected three-pad algorithm is small, though noticeable. In contrast, imposing a fixed width of $\tilde{\sigma}$ seriously degrades the resolution. This is shown in Figs. 5, 6.

Resolution from the Three-Pad Algorithm

Using the fitted σ (i.e., Eq. 7 from SN0137) and plotting the resolution for $w = 0.67$ cm and $\Delta h/h_c = 0.05$, one obtains the zero-diffusion curves for Δx in Fig. 7. These are similar to Fig. 2 in SN0137. If diffusion effects are calculated, one must compensate for the reduced effective

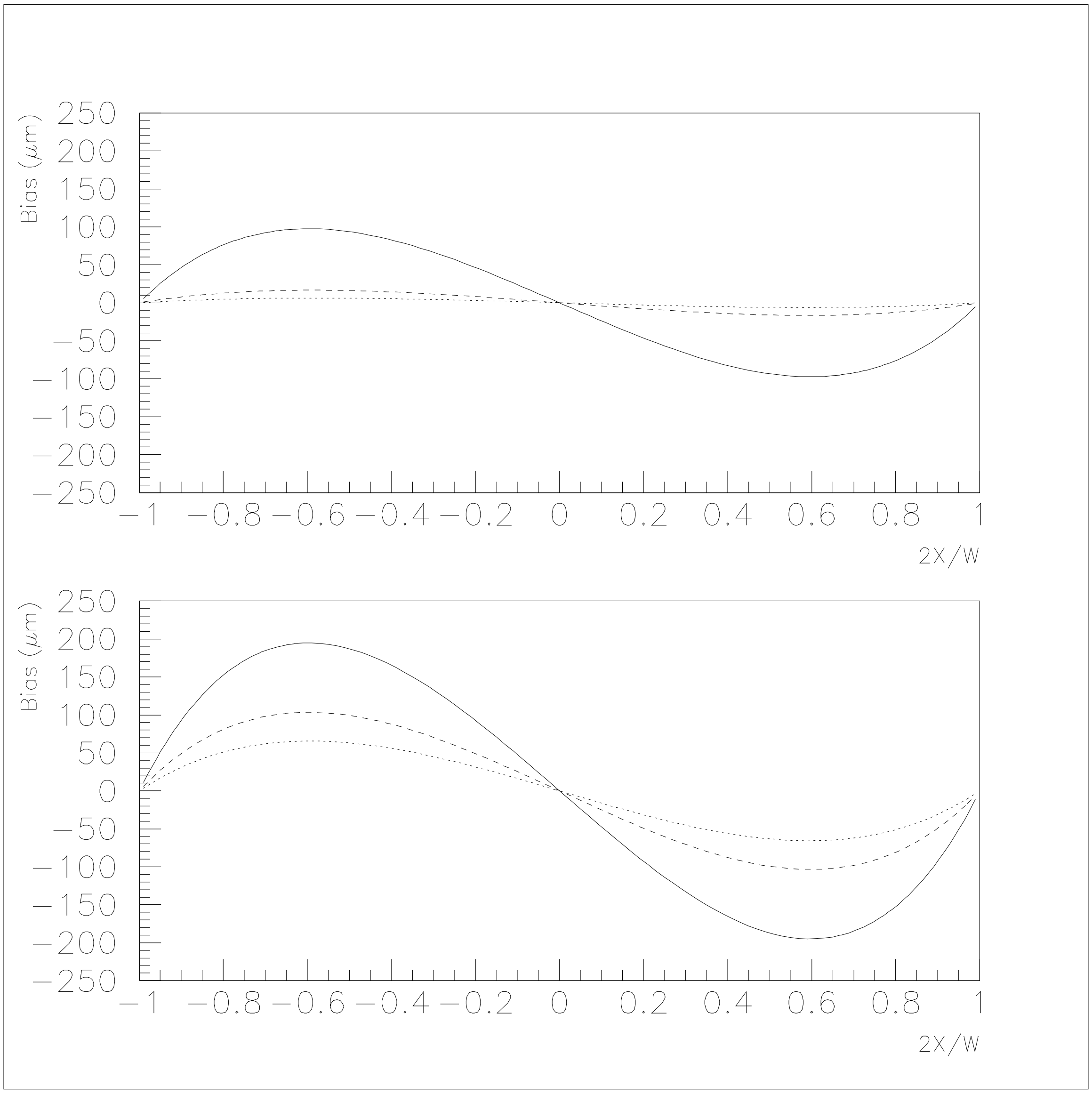

Figure 3: Position bias for tracks of zero crossing angle with the three-pad algorithm when the fitted σ is used. a) Inner pads; b) outer pads. The curves represent $\sigma_{\rm dif} = 0$ (solid line), $\sigma_{\rm dif} = 0.185$ cm (dashed line) and $\sigma_{\rm dif} = 0.262$ cm (dotted line).

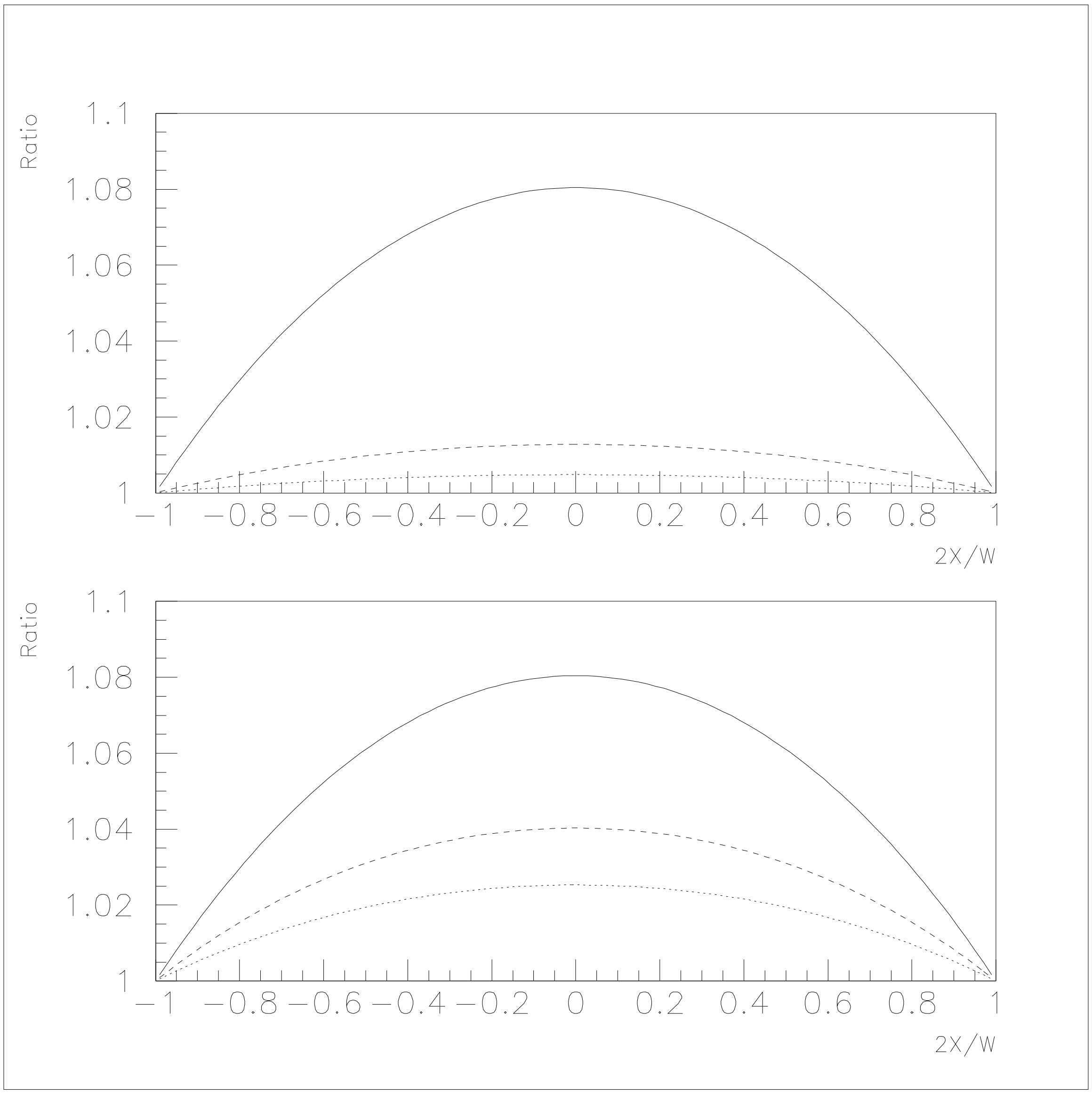

Figure 4: Ratio of $\tilde{\sigma}/\sigma$ (ideal over fitted) for tracks of zero crossing angle with the three-pad algorithm. a) Inner pads; b) outer pads. The curves are for $\sigma_{\rm dif} = 0$ (solid line), $\sigma_{\rm dif} = 0.185$ cm (dashed line) and $\sigma_{\rm dif} = 0.262$ cm (dotted line).

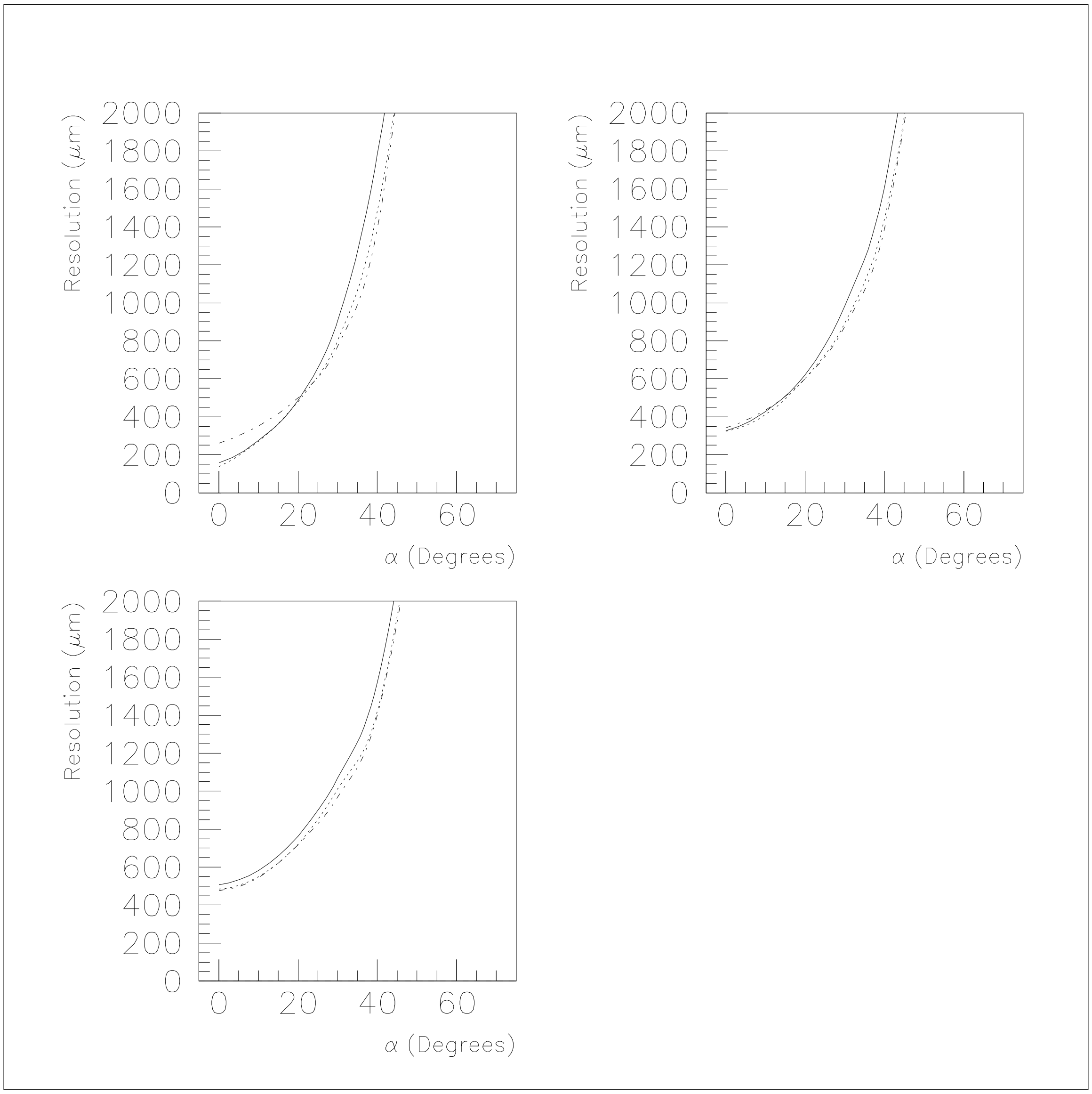

Figure 5: Monte Carlo resolution for the inner TPC versus track crossing angle α from the three-pad algorithm using the fitted width σ (solid lines), calculated width $\tilde{\sigma}(x)$ (dot-dash lines) and a scaling of the fitted width (dotted lines). The figures are for a) $\sigma_{\rm dif} = 0$, b) $\sigma_{\rm dif} = 0.185$ cm and c) $\sigma_{\rm dif} = 0.262$ cm.

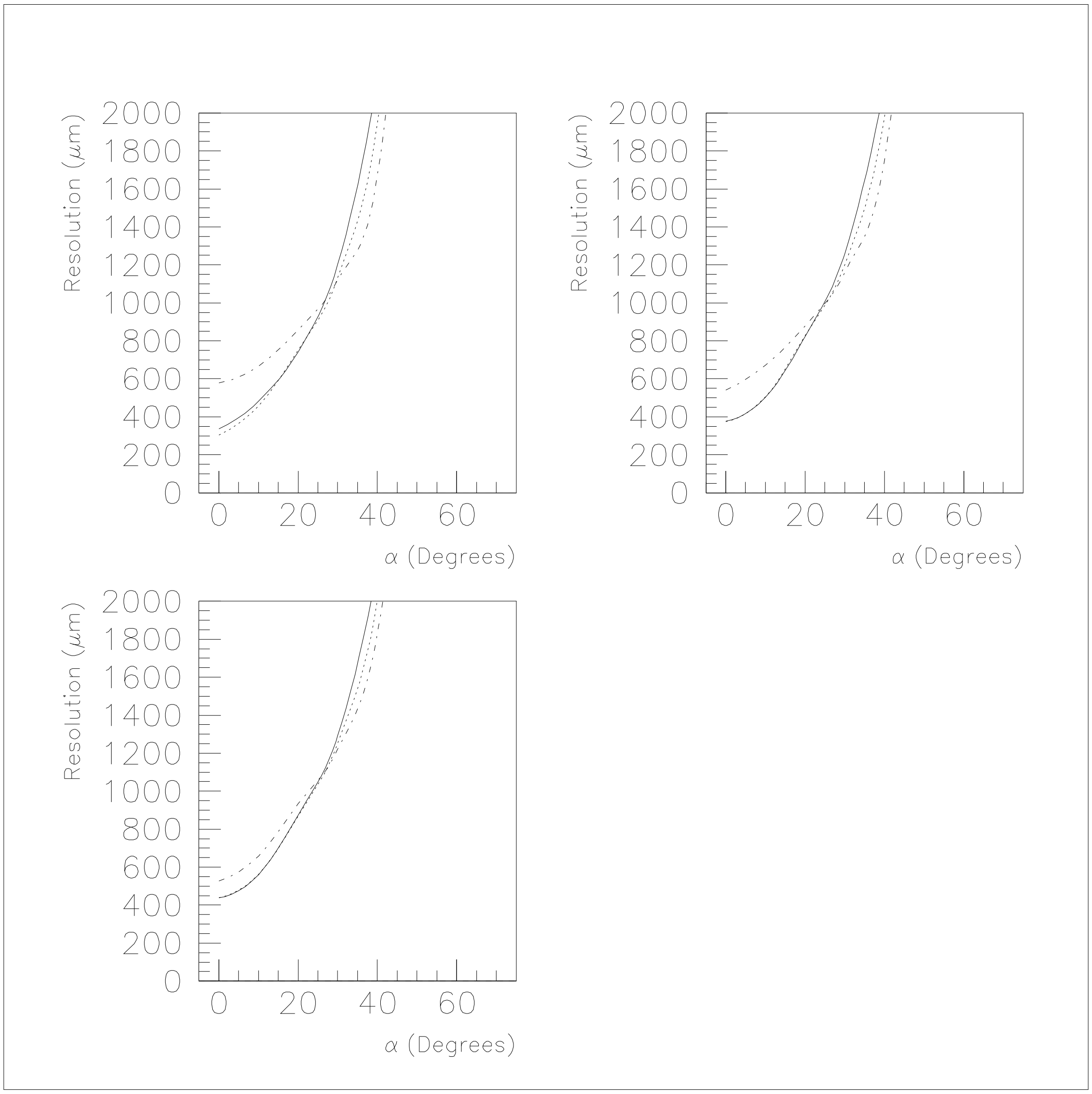

Figure 6: Example of Monte Carlo resolution for the outer TPC versus track crossing angle α from the three-pad algorithm using the fitted width σ (solid lines), calculated width $\tilde{\sigma}(x)$ (dot-dash lines) and a scaling of the fitted width (dotted lines). The figures are for a) $\sigma_{\mathrm{dif}} = 0$, b) $\sigma_{\mathrm{dif}} = 0.185$ cm and c) $\sigma_{\mathrm{dif}} = 0.262$ cm.

coupling to the central pad (by increasing $\Delta h/h_c$) to make a fair comparison. Figure 7 does *not* include the statistical aspects of ionization and diffusion, which further reduce resolution, nor does it include crossing-angle effects.

The average noise in the front-end electronics (FEE) is equivalent to 940 e^-, with a maximum of 1110 e^-, at an input capacitance of 30 pF.[11] On average, the smallest signals will be produced by minimum-ionizing tracks, perpendicular to the beam axis and at zero crossing angle. For P10, the average ionization is ~90 ion pairs/cm, but, for a step size of 1.2 cm, the main distribution is ~0.51% of the average; at 2.0 cm, it is ~53%. Again, the wire-pad couplings have been measured as 0.30 (inner) and 0.34 (outer). For pad lengths L_y of 1.2 cm (inner) and 2.0 cm (outer):

$$\left(\frac{\Delta h}{h_c}\right)_{\text{inner}} \approx \frac{940\ \text{e}^-}{0.51 \times 90\ \text{e}^-/\text{cm} \times 1.2\ \text{cm} \times 0.30 \times G_{\text{inner}}} = \frac{56.9}{G_{\text{inner}}}$$

and

$$\left(\frac{\Delta h}{h_c}\right)_{\text{outer}} \approx \frac{940\ \text{e}^-}{0.53 \times 90\ \text{e}^-/\text{cm} \times 2.0\ \text{cm} \times 0.34 \times G_{\text{outer}}} = \frac{29.0}{G_{\text{outer}}} .$$

G_{inner} and G_{outer} are the inner and outer gas gain, respectively.

The CDR Update (Eq.4C-5) gives the spatial resolution for isolated tracks as

$$\sigma_{\text{res}}^2 = \sigma_A^2 + \sigma_B^2 L e^{\gamma L} \sec\alpha + \sigma_C^2 e^{\gamma L} \cos\alpha \tan^2\alpha ,$$

where L is the drift length, and γ is the attenuation constant. The base resolutions (zero diffusion, zero crossing angle) are $\sigma_A = 135\ \mu$m (inner) and $\sigma_A = 303\ \mu$m (outer). The gains required to achieve this resolution can be estimated from Fig. 7 (which assumed $\Delta h/h_c = 0.05$), in which the solid lines in Fig. 7 average to 160 μm (inner) and 320 μm (outer):

$$G_{\text{inner}} = \frac{56.9}{0.05} \cdot \frac{160\ \mu\text{m}}{135\ \mu\text{m}} = 1138 \cdot 1.19 = 1350 \ \text{ and}$$

$$G_{\text{outer}} = \frac{29.0}{0.05} \cdot \frac{320\ \mu\text{m}}{303\ \mu\text{m}} = 580 \cdot 1.06 = 615 .$$

These gains and a 940 e^-/pad noise were used in a Monte Carlo in which the three-pad algorithm bias was corrected by scaling σ; other assumptions are listed in Table 1. The calculated resolutions were remarkably close to the CDR values: $\sigma_A = 137\ \mu$m (inner) and $\sigma_A = 305\ \mu$m (outer). The uncorrected 3-pad algorithm would require gains 10–15% higher.

The higher gain for the inner pads is easily understood: the average ionization signal on the pad row is smaller by a factor of (1.2 cm)/(2.0 cm)=0.60; the main ionization distribution relative to the average is lower by a factor of 0.51/0.53=0.96; the pad coupling is smaller by a factor of 0.30/0.34=0.88; and the specified resolution relative to pad width is tighter by a factor of $\frac{135}{0.335}/\frac{303}{0.670} = 0.89$. Taken together, these correctly predict that the inner gain must be higher by a factor of 2.20 to meet the CDR base resolution values.

[11] S. R. Klein et al., LBL-37904 (1995).

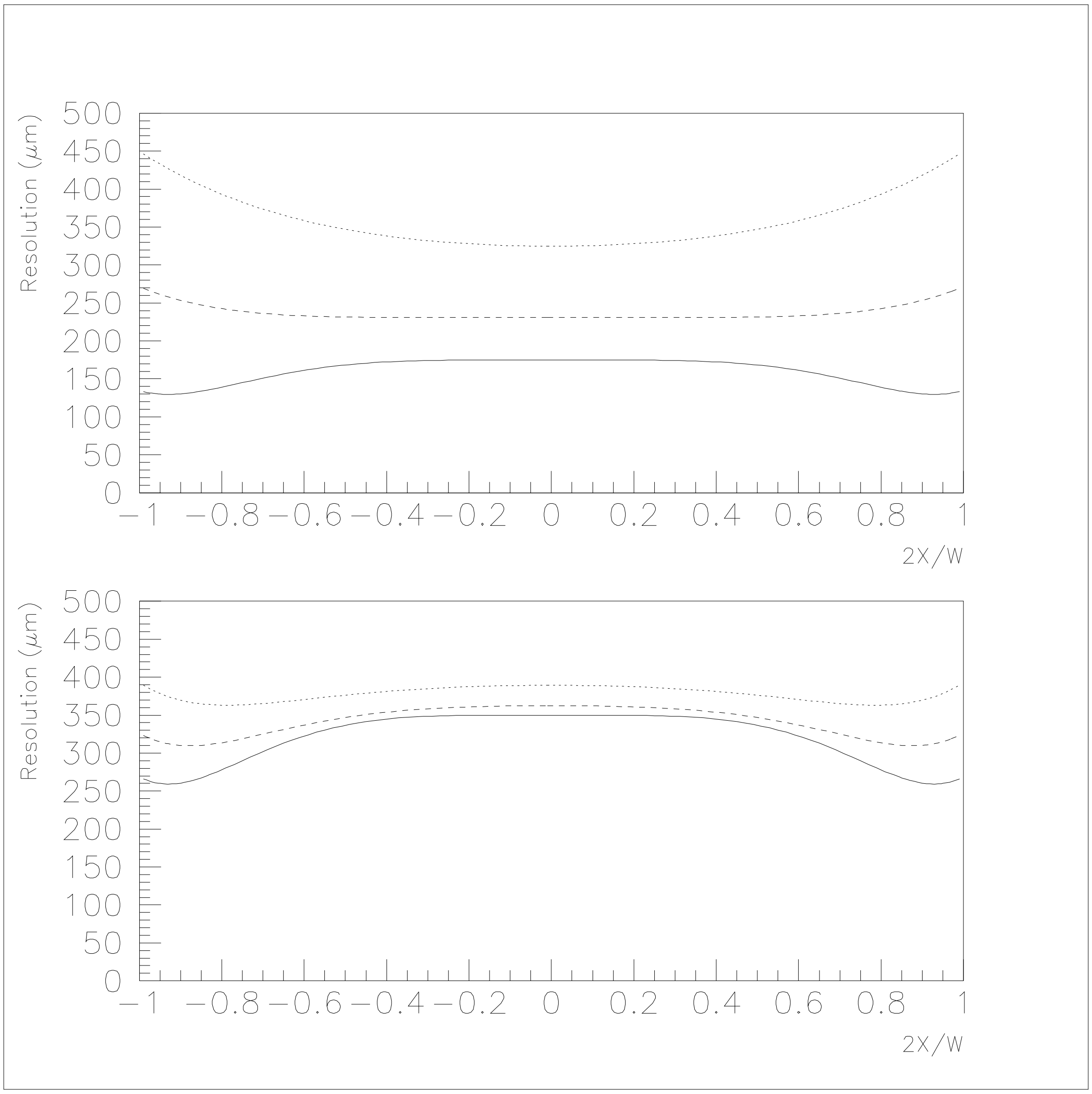

Figure 7: Resolution from the three-pad algorithm at zero crossing angle in the absence of statistical fluctuations other than noise: a) inner pads; b) outer pads. In each plot, the curves are for $\sigma_{\rm dif} = 0$ (solid line), $\sigma_{\rm dif} = 0.185$ cm (dashed line) and $\sigma_{\rm dif} = 0.262$ cm (dotted line). The signal and noise are such that $\Delta h/h_c$=0.05 for $\sigma_{\rm dif} = 0$.

Gas composition	P10
Gas pressure (bar)	1.0
Gas temperature (°C)	23.9
Transverse diffusion (μm/cm$^{1/2}$)	185
Noise (e$^-$ equivalent)	940
Threshold (counts)	3.0
Gain-selection bin width	5%
G_{inner}	1350
G_{outer}	615
L_y (inner, cm)	1.2
L_y (outer, cm)	2.0
w (inner, cm)	0.335
w (outer, cm)	0.670

Table 1: Conditions used for the resolution simulations reported in this note.

Digitization Error

Ideally, digitization error is a constant $1/\sqrt{12}$ channel; at 0.12 fC/channel for the TPC FEE, this is equivalent to a 217 e$^-$ noise. This is further reduced because a signal is spread over several pixels. In all cases, it will be negligible compared to the electronics noise. Though the 10-to-8-bit compression will make large-signal bins wider, the loss of resolution will still be tiny.[12]

Effect of Amplifier Gain Variation

The FEE amplifier gains will be trimmed into 5% bins; the rms gain variation should be $5\%/\sqrt{12}$=1.44%. If these gain variations are random and $\Delta h/h_c \approx 5\%$, there would be little additional resolution loss. Equation 8 from SN0137 can be rewritten as

$$\Delta x = \frac{1}{\sqrt{2}}\frac{\Delta G}{G}\frac{\sigma^2}{w}\left[1+3\left(\frac{2x}{w}\right)^2\right]^{1/2} ,$$

where G and ΔG are the gain and its rms variation, respectively. Assuming 5% gain bins, the average over x is

$$\Delta x = 0.976\frac{\Delta G}{G}\frac{\sigma^2}{w} = 0.0141\frac{\sigma^2}{w} .$$

Applying the pad response function width from Fig. 1b ($\sigma/w = 0.602$) gives

$$\Delta x = 0.0141\frac{\sigma^2}{w} = 0.0141 \cdot 0.602^2 w = 0.0051w .$$

[12]Star Note SN0116, R. Bossingham.

The resulting Δx=17 μm (inner) and Δx=34 μm (outer) broadens the resolution by only 1% for $\sigma_A = 135$ μm (inner) and $\sigma_A = 303$ μm (outer). The gain variation was incorporated into the Monte Carlo studies for this note, but the effect was tiny.

Ionization Statistics

For thin volumes, such as a few centimeters of P10 at atmospheric pressure, the most probable number of ion pairs is considerably below the average. In addition, the distribution is wide, asymmetric and cannot be described by a simple formula. However, a Monte Carlo treatment incorporating empirical results *is* simple to code.

Empirical results exist for primary ionizations per centimeter[13 14] and for the cluster-size distributions in argon and methane.[15] It is not strictly correct to add these distributions linearly to simulate an argon-methane mixture, but the approximation is accurate at the 1–2% level. (The metastable excitation level of argon falls below the ionization potential of methane, so true Penning effect cannot occur in P10.) In any case, the F. Rieke *et al.* results were deconvoluted from measurements that were actually done with an argon-methane mixture. These results formed the primary input for the cluster model Monte Carlo used in this note. More detailed information about this algorithm, including comparisons with the Geant 3.21 photo-absorbtion ionization (PAI) algorithm, are given in SN0249.[16]

As discussed above, the ionization distribution is such that the effective noise-to-signal ratio is increased by a nearly a factor of two in the STAR TPC. For a fixed gain, this reduces the base resolution σ_A by nearly the same factor.

The diffusion term in the resolution ($\sigma_B\sqrt{L}$, where L is the drift length) is also increased by the reduced electron statistics. We have already shown the effect due to the reduction in the signal and its broadening in Fig. 7, but that is just the noise effect with a specific algorithm. There is a genuine loss of information, since part of the signal spreads onto more pads with additional, independent noise, but Fig. 7 also reflects the fact that the algorithm uses only three pads.

The effect of electron statistics is especially noticeable for the inner subsector. From the discussions above, this should be

$$\sigma_B\ (\text{inner}) = \frac{1850\ \mu\text{m}}{\sqrt{\text{m}}} \cdot \frac{1}{\sqrt{0.51 \cdot (90/\text{cm}) \cdot (1.2\ \text{cm})}} = \frac{249\ \mu\text{m}}{\sqrt{\text{m}}} \quad \text{and}$$

$$\sigma_B\ (\text{outer}) = \frac{1850\ \mu\text{m}}{\sqrt{\text{m}}} \cdot \frac{1}{\sqrt{0.53 \cdot (90/\text{cm}) \cdot (2.0\ \text{cm})}} = \frac{189\ \mu\text{m}}{\sqrt{\text{m}}} .$$

[13] F. Rieke andW. Prepejchal, Phys. Rev. A**6**, 1597 (1972).

[14] A. Pansky, G. Malamud, A. Breskin and R. Chechik, NIM **A**323, 294 (1992).

[15] H. Fischle, J. Heintze and B. Schmidt, NIM **A**301, 202 (1991).

[16] STAR Note SN0247, R. Bossingham (1996).

These values are only slightly larger than those quoted in the STAR CDR Update (213 μm and 166 μm) because that work assumed 2330 $\mu\mathrm{m}/\sqrt{\mathrm{m}}$ for the single-electron transverse diffusion. The values parametrized from simulations are similar, though the exact values are algorithm-dependent.

Crossing Angle

It is clear that the effective pad response function becomes non-Gaussian for tracks at a large crossing angle. For a pad length L_y, the effect should become significant when $L_y \tan\alpha/\sqrt{12}$ is of order σ. For the outer pad rows, $L_y = 2$ cm and $\sigma = 0.48$ cm in P10 for hits drifting from the membrane. Therefore, one expects the effect to be important for $\alpha > 40°$; the three-pad resolution in Figs. 5, 6 does, in fact, degenerate rapidly above 40°. By 70°, the charge distribution is so wide that the three-pad algorithm becomes unstable with 32-bit calculation, even in the absence of noise. To give some idea of the range of interest, α is plotted in Fig. 8 at the center and ends of several pad rows as a function of transverse momentum.

Double Two-Pad Algorithm

In Blum and Rolandi's discussion[17] of TPC pad information, they note that

> [the three-pad algorithm] can be also used to derive a measurement of x *independent* of the a priori knowledge of the pad response function s. In practical cases this is not convenient since one obtains a better resolution if one uses a known parameterization of s^2.

Their suggestion is to use a weighted average of two, two-pad estimates:

$$x = x_i + w\left[\frac{h_{i-1}^2}{h_{i-1}^2 + h_{i+1}^2}\left(\frac{s^2}{w^2}\ln\frac{h_i}{h_{i-1}} - \frac{1}{2}\right) + \frac{h_{i+1}^2}{h_{i-1}^2 + h_{i+1}^2}\left(\frac{s^2}{w^2}\ln\frac{h_{i+1}}{h_i} + \frac{1}{2}\right)\right] .$$

Obtaining the "known parameterization of s^2" requires global information (i.e., the crossing angle), implying a second tracking pass (anticipated, but not implemented, for the STAR TPC software). The same is also true of correcting the three-pad algorithm bias. On the other hand, an estimate of crossing angle can be obtained from the cluster shape,[18] so this algorithm might be useful, even for the first pass. Its resolution is compared against that of the bias-corrected three-pad algorithm in Figs. 9, 10, assuming that the crossing angle, diffusion and intrinsic pad response function are known for both algorithms. On the whole, the Blum and Rolandi algorithm is slightly better, but not by more than 10%.

[17] *Particle Detection with Drift Chambers*, W. Blum and L. Rolandi, published by Springer-Verlag, 1993, p.163.

[18] STAR Note SN0238, M. Lisa.

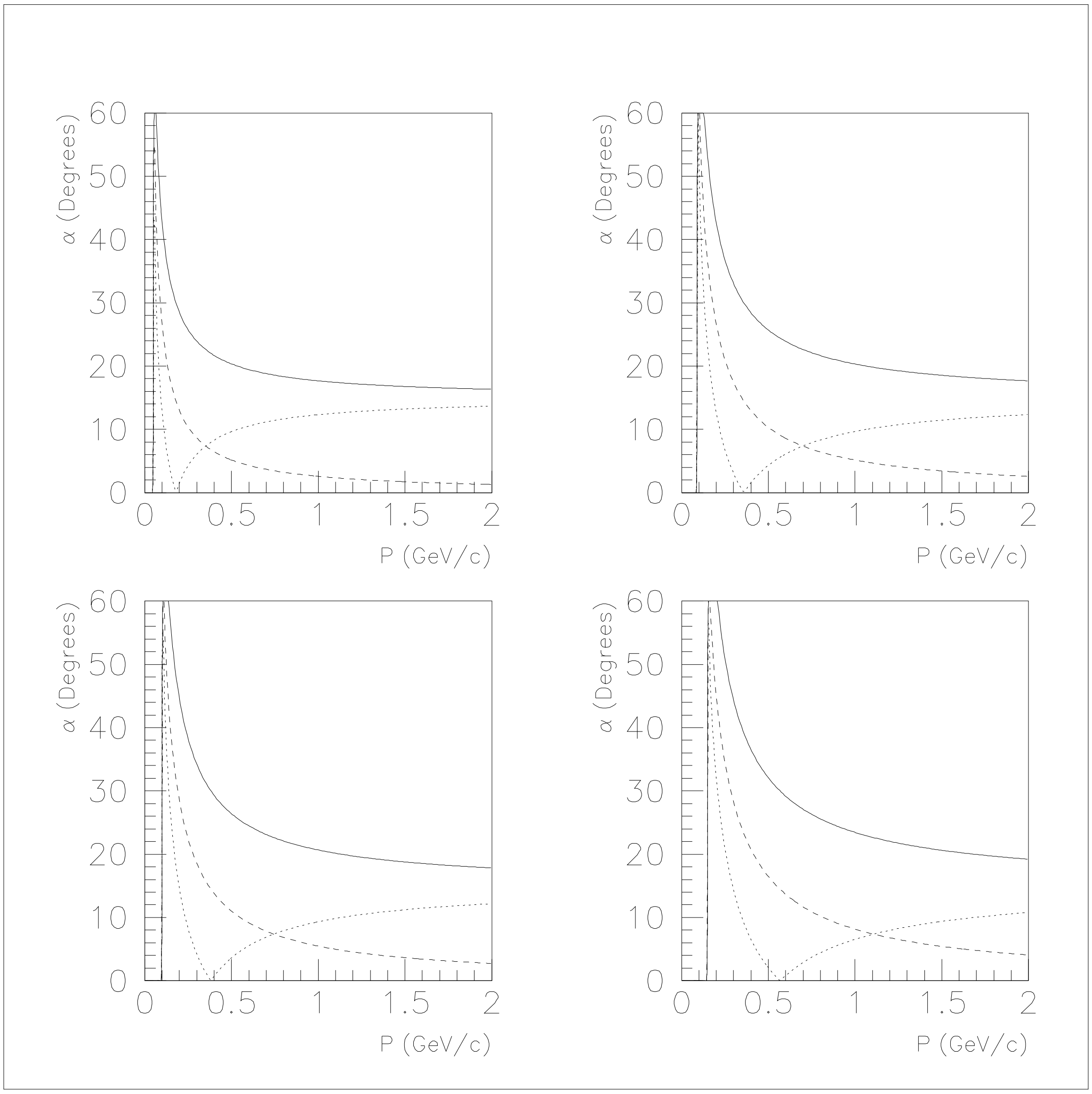

Figure 8: Crossing angle as a function of transverse momentum for the 15° pads at either end of a pad row (solid and dotted lines) and the 0° pad at the center (dashed line): a) pad row 1; b) pad row 13 (last inner row); c) pad row 14; and d) pad row 45 (last outer row). Tracks were propagated from the TPC center without energy loss or scattering.

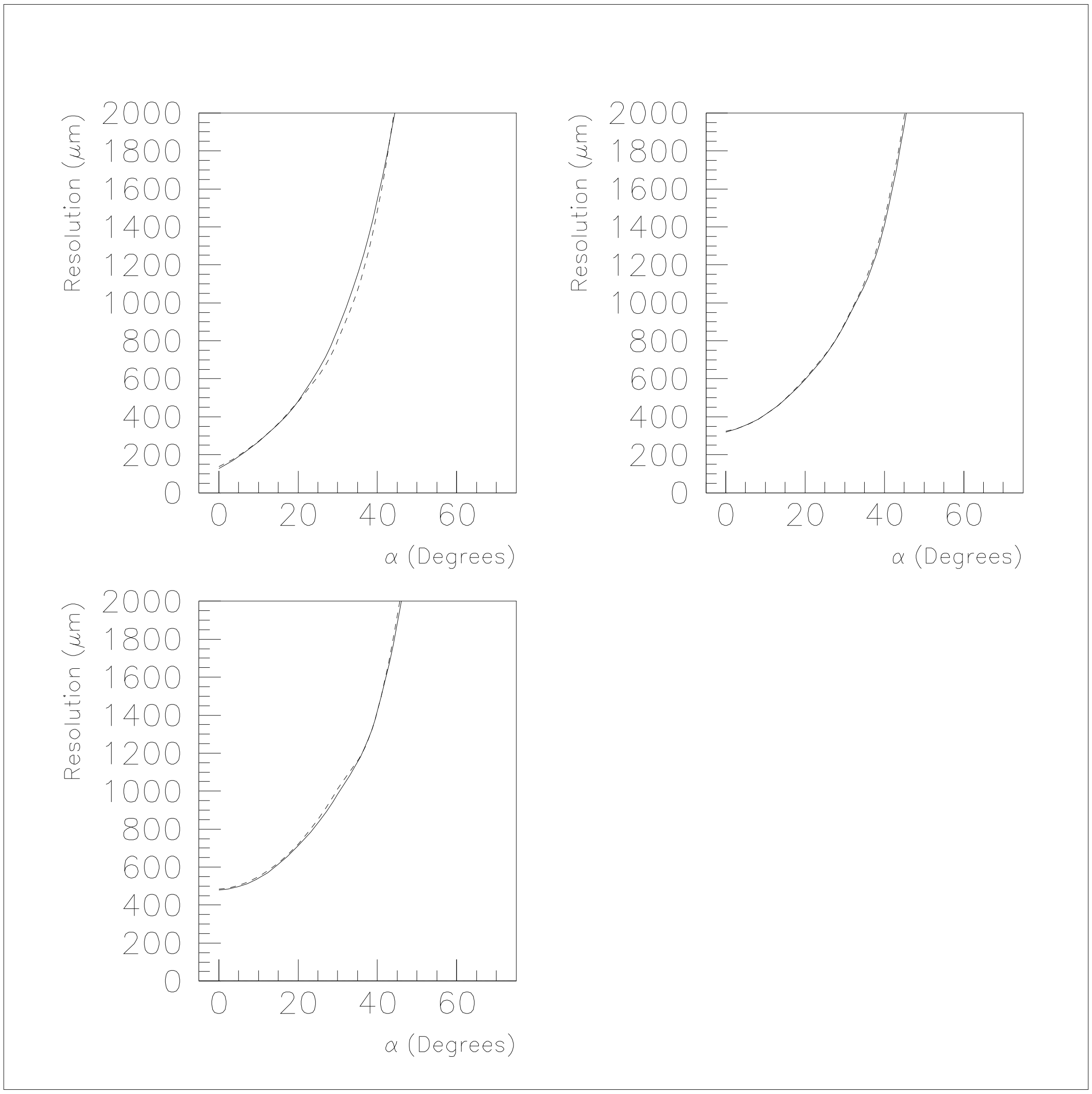

Figure 9: Comparison of calculated resolution for the double two-pad algorithm (solid lines) and three-pad algorithm with bias correction (dashed lines) versus crossing angle for the inner TPC. The figures are for a) $\sigma_{\rm dif} = 0$ (solid line), b) $\sigma_{\rm dif} = 0.185$ cm (dashed line) and c) $\sigma_{\rm dif} = 0.262$ cm (dotted line). Crossing angle, diffusion and intrinsic pad response were assumed for both algorithms.

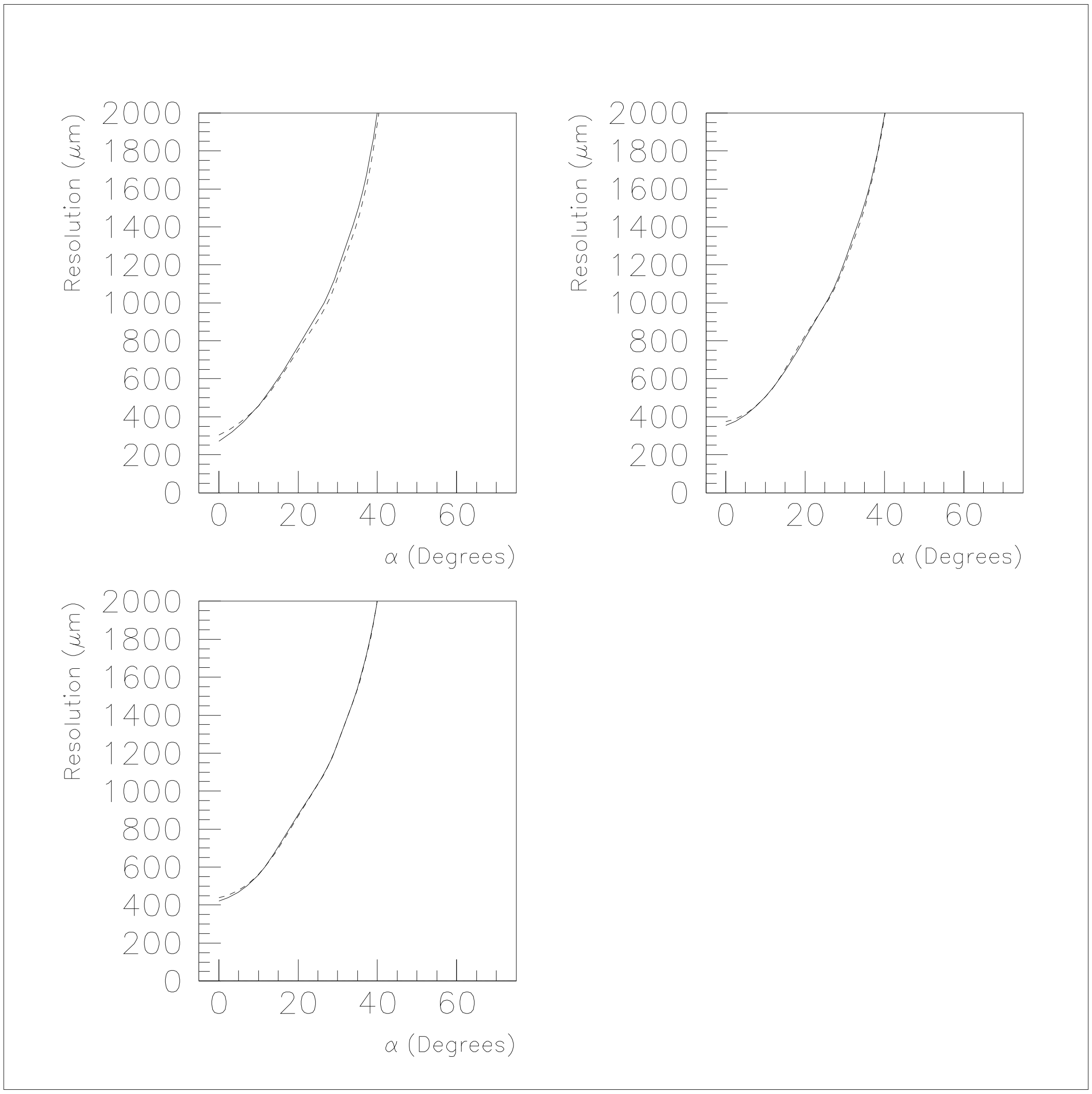

Figure 10: Comparison of resolution for the double two-pad algorithm (solid lines) and three-pad algorithm with bias correction (dashed lines) versus crossing angle for the outer TPC. The figures are for a) $\sigma_{\mathrm{dif}} = 0$ (solid line), b) $\sigma_{\mathrm{dif}} = 0.185$ cm (dashed line) and c) $\sigma_{\mathrm{dif}} = 0.262$ cm (dotted line). Crossing angle, diffusion and intrinsic pad response were assumed for both algorithms.

Weighted-Mean Algorithm

Any algorithm using only three central pads will deteriorate at large crossing angles. A simple weighted-mean algorithm using all contiguous pads above threshold will eventually give better results; this is compared to the double two-pad algorithm in Figs. 11, 12. It gives significantly better resolution above 22° in the inner TPC and above 30° in the outer TPC.

Four-Pad, Five-Pad and "Best" Algorithms

When a significant signal is induced on more than three pads, improved resolution may be achieved with a four- or five-pad algorithm. A simple implementation combines the two peak pads (four-pad algorithm) or the pair on either side of the peak pad (five-pad algorithm), then proceeds as for the three-pad algorithm. Trivial changes compensate for the different geometry; biases are corrected by scaling the fitted width.

Even three pads do not always exceed threshold for a hit, and algorithms using more pads are not useful if the additional pads do not carry information. At short drift distances, the charge distribution is unspread by diffusion, so the four- and five-pad algorithms are only useful for atypically large signals. This makes it somewhat misleading to plot their resolution. Instead, Figs. 13, 14 display the resolution for the best of the applicable, studied algorithms—where "best" means the best resolution for a distribution of tracks at that crossing angle, drift distance and TPC subsector.

The resolution could undoubtedly be improved by choosing the "best" algorithm event by event, based on a knowledge of the pad signals and noise. Similarly, a bit more information might be wrung from an event by taking a weighted mean of multiple algorithms, but this requires a knowledge of the correlations between the various algorithms. Neither approach has been studied in detail, but preliminary trials showed some improvement. (The real "best" values would come from a maximum-likelihood fit, but the computation cost precludes this.)

Finally, Fig. 15 compares the "best" algorithm resolution as a function of crossing angle for the inner and outer TPC, and for several drift distances. The smaller pad size in the inner TPC gives a better resolution except for very long drift distances; then, diffusion spreads the signal over several pads, decreasing the signal:noise ratio.

Resolution Parameterization

Recall again the CDR formula for isolated hit resolution :

$$\sigma_{\rm res}^2 = \sigma_A^2 + \sigma_B^2 L e^{\gamma L} \sec\alpha + \sigma_C^2 e^{\gamma L} \cos\alpha \tan^2\alpha \ ,$$

The constants from the CDR update are listed in Table 2.

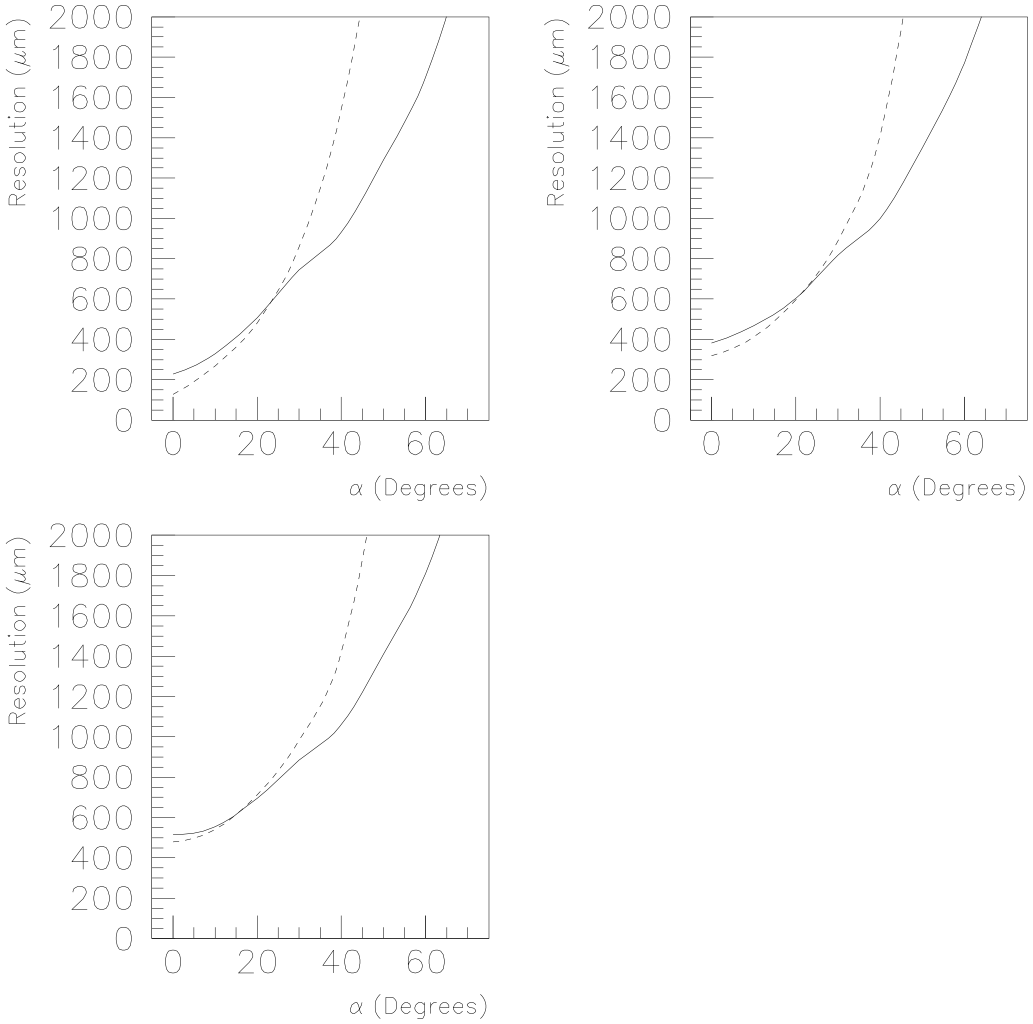

Figure 11: Comparison of calculated resolution for the weighted-mean algorithm (solid lines) and double two-pad algorithm (dashed lines) versus crossing angle for the inner TPC. The figures are for a) $\sigma_{\text{dif}} = 0$ (solid line), b) $\sigma_{\text{dif}} = 0.185$ cm (dashed line) and c) $\sigma_{\text{dif}} = 0.262$ cm (dotted line). Crossing angle, diffusion and intrinsic pad response were assumed only for the double two-pad algorithm.

	Inner Pads	Outer Pads
σ_A	135 μm	303 μm
σ_B	213 μm	166 μm
σ_C	1000 μm	1665 μm

Table 2: Resolution coefficients from the STAR CDR Report Update.

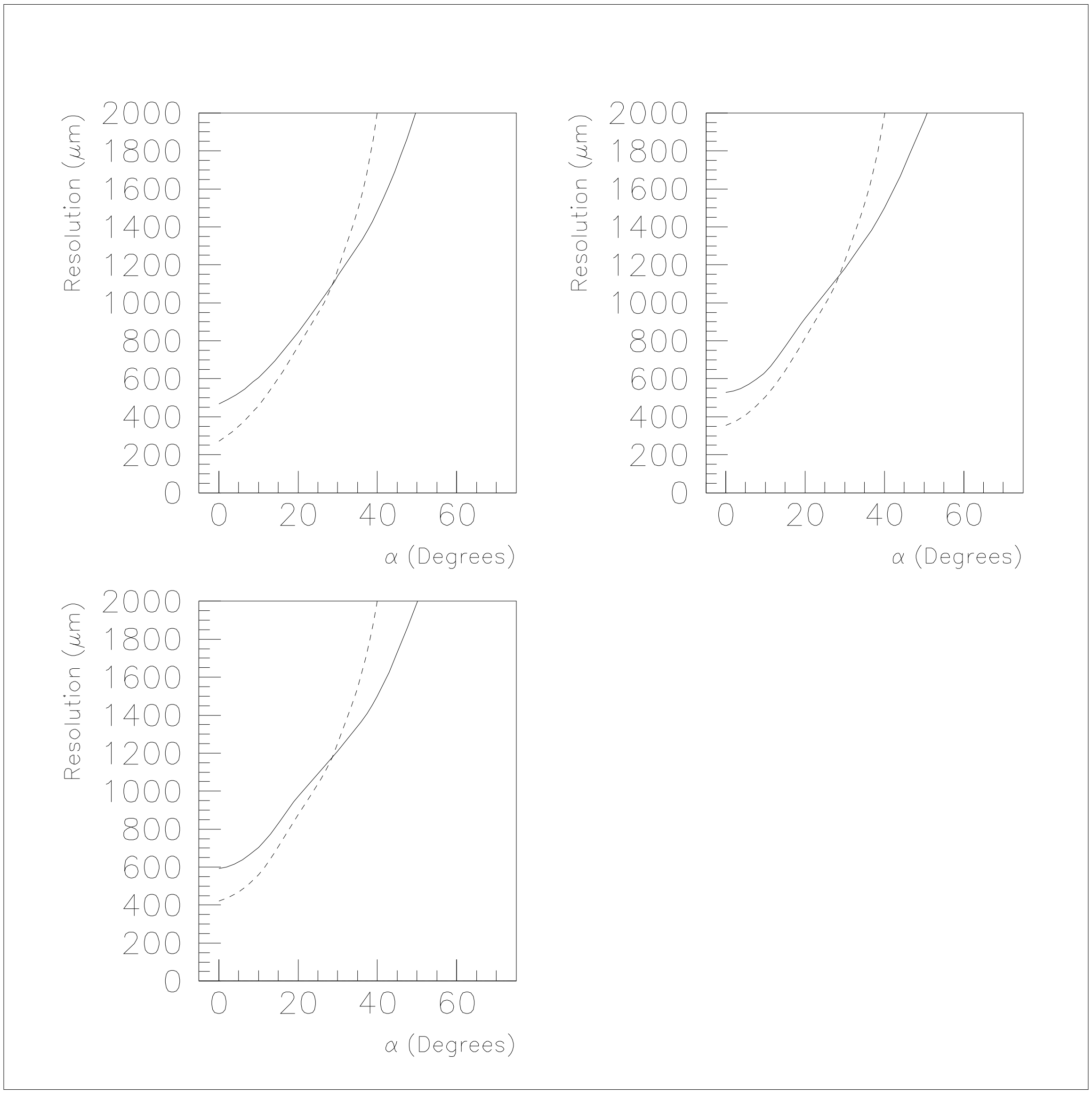

Figure 12: Comparison of resolution for the weighted-mean algorithm (solid lines) and double two-pad algorithm (dashed lines) versus crossing angle for the outer TPC. The three figures are a) $\sigma_{\rm dif} = 0$ (solid line), b) $\sigma_{\rm dif} = 0.185$ cm (dashed line) and c) $\sigma_{\rm dif} = 0.262$ cm (dotted line). Crossing angle, diffusion and intrinsic pad response were assumed only for the double two-pad algorithm.

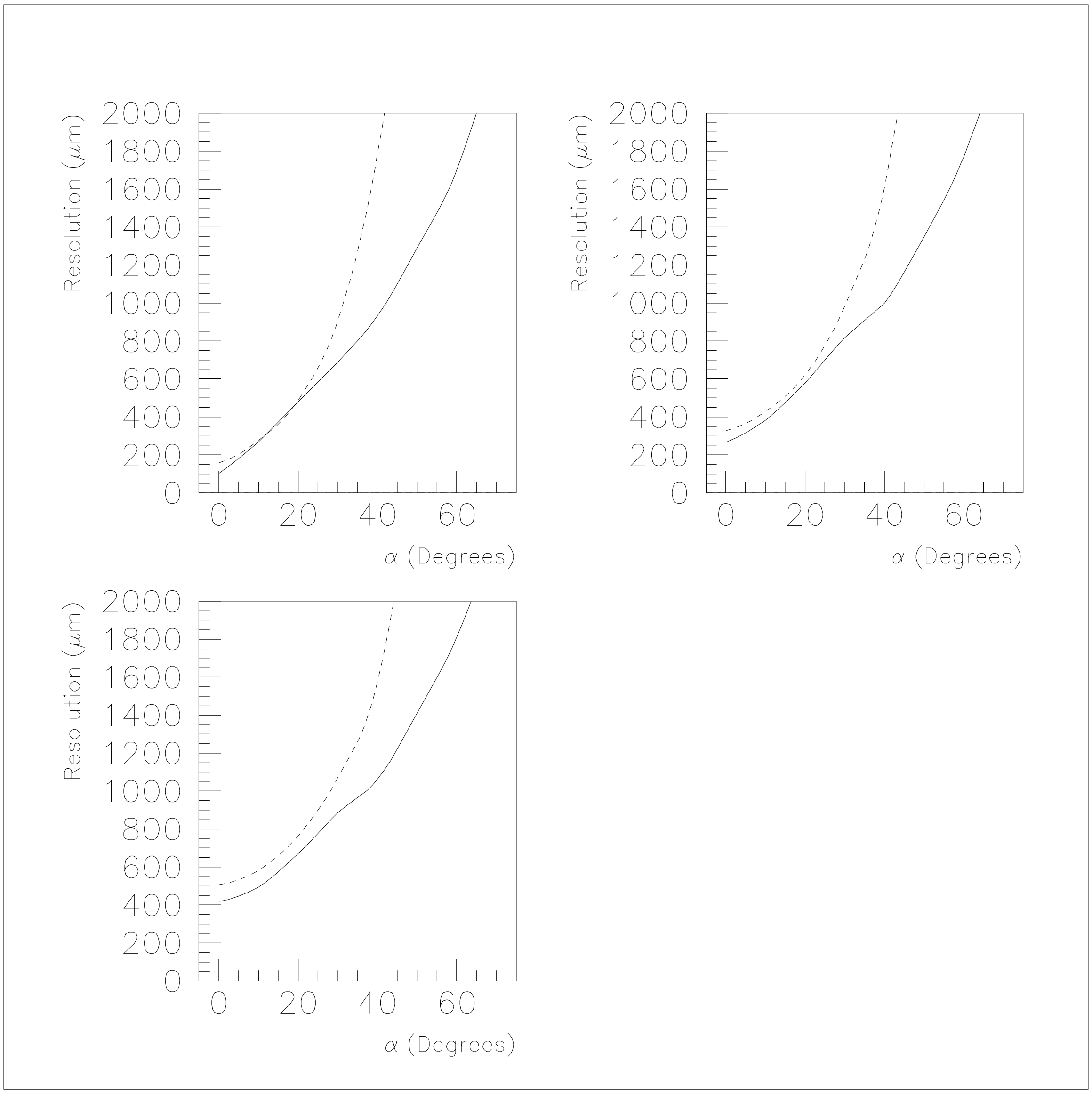

Figure 13: R-ϕ resolution in the inner TPC versus crossing angle with the "best" algorithm (solid line) and uncorrected three-pad algorithm (dashed line); the plots correspond to transverse diffusion widths of a) $\sigma_{\rm dif} = 0$, b) $\sigma_{\rm dif} = 0.185$ cm and c) $\sigma_{\rm dif} = 0.262$ cm.

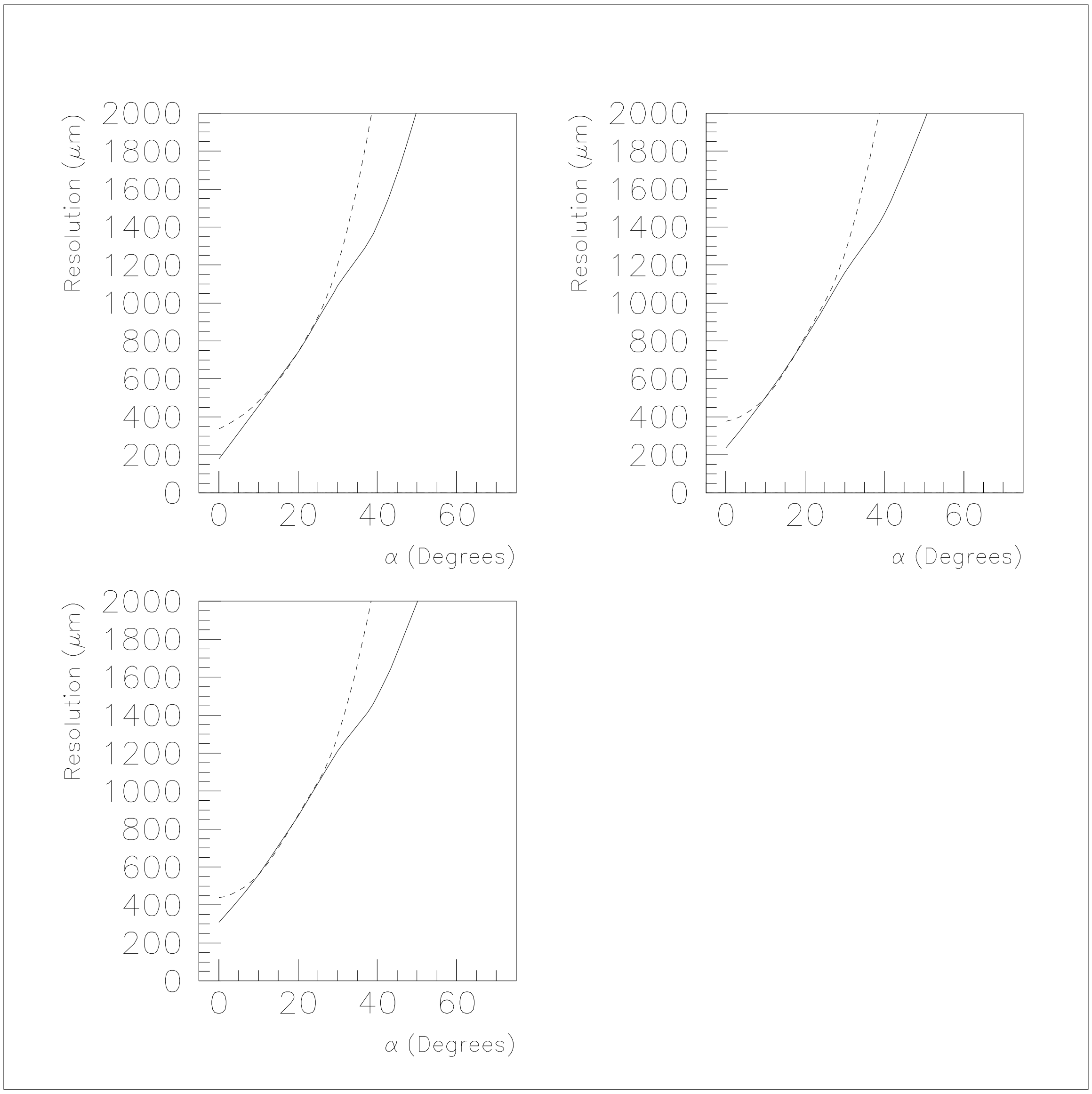

Figure 14: R-ϕ resolution in the outer TPC versus crossing angle with the "best" algorithm (solid line) and uncorrected three-pad algorithm (dashed line); the plots correspond to transverse diffusion widths of a) $\sigma_{\rm dif} = 0$, b) $\sigma_{\rm dif} = 0.185$ cm and c) $\sigma_{\rm dif} = 0.262$ cm.

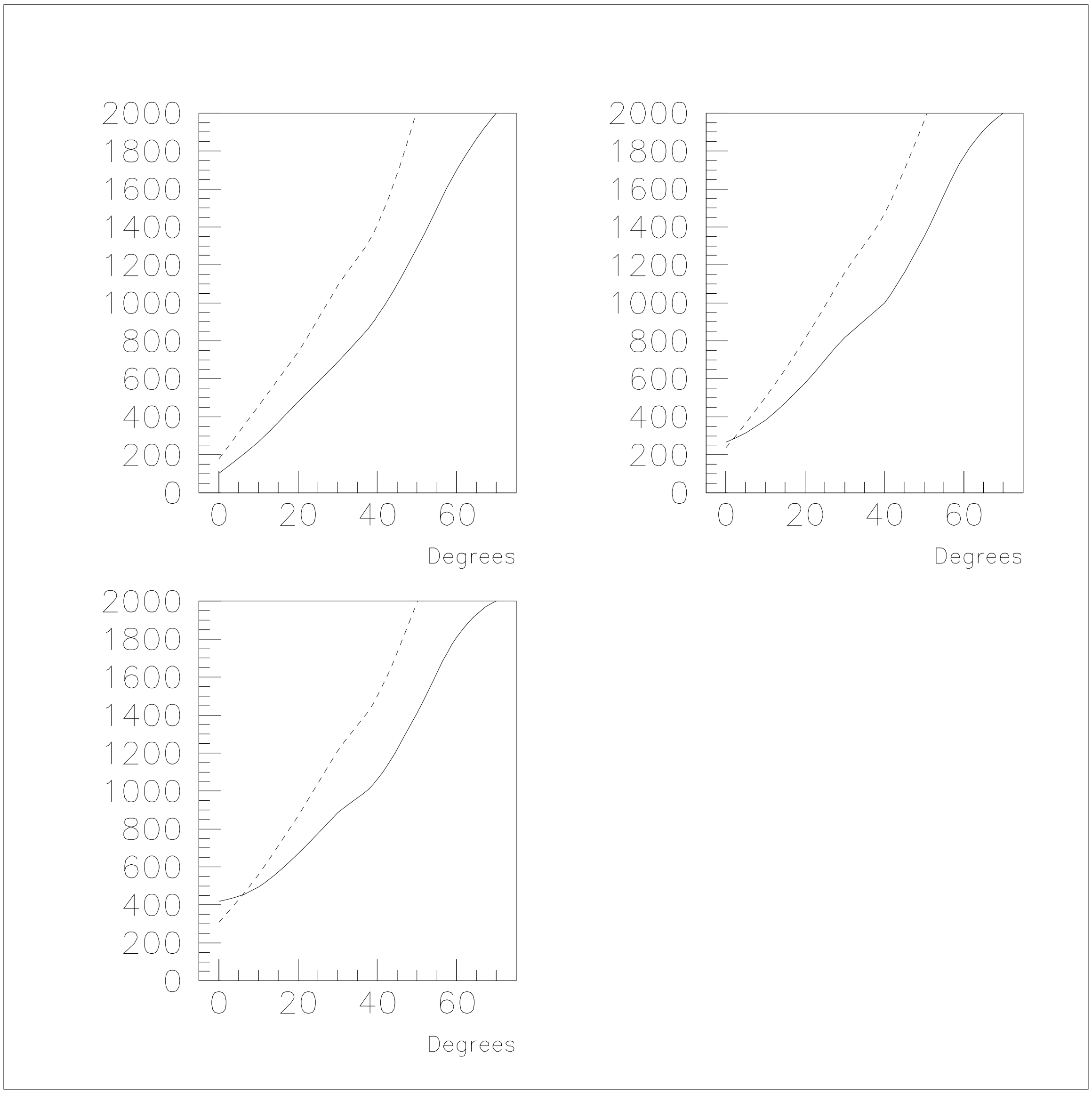

Figure 15: "Best" resolution versus crossing angle in the inner (solid line) and outer (dashed line) TPC. The figures are for a) $\sigma_{\rm dif} = 0$, b) $\sigma_{\rm dif} = 0.185$ cm and c) $\sigma_{\rm dif} = 0.262$ cm.

For comparison, the results in Fig. 15 are parametrized in Table 3. Note that σ_A is close to being inversely proportional to gain, as long as noise dominates the resolution. Since the gas gain in the simulation was adjusted to match the CDR σ_A's with the corrected three-pad algorithm, the reduction relative to Table 2 is solely due to the use of a different algorithm.

	Inner Pads	Outer Pads
σ_A	117 μm	212 μm
σ_B	270 μm	190 μm
σ_C	1300 μm	2000 μm

Table 3: Pad resolution coefficients calculated for minimum-ionizing tracks in P10 using the "best" algorithm at each drift distance and crossing angle, assuming 940 e^- noise, 5% gain-selection bins, $G_{\text{inner}} = 1350$, and $G_{\text{outer}} = 615$.

Clearly, the σ_A's could be reduced further by increasing gas gain, but at the cost of reduced dynamic range. In any case, there is little point in lowering it far below the resolutions obtainable at moderate crossing angles and drift distances. A high-momentum hit with a 1-m drift length, 7.5° crossing angle and σ_A as in Table 3 has a resolution of 340 μm (inner) or 390 μm (outer). If the base resolution were zero, both values would decrease to 320 μm. Similarly, for pads with the maximum capacitance (1110 e^- noise) the values would increase to only 350 μm (inner) and 410 μm (outer).

The σ_A's become even less important for tracks with non-zero pitch angles, since the ionization on a pad will be increased; σ_B and σ_C will also be reduced for non-zero pitch angles, but those effects will be smaller. For example, $\sigma_B \propto \sqrt{\sin\theta}$, where $90 - \theta$ is the pitch angle.

Finally, it must be said that the σ_B'c and σ_C'c in Table 3 may be slight overestimates, viewed globally. Howard Wieman has noted that, since the resolution was calculated for a single pad row, the anticorrelation between hits in adjacent rows due to charge sharing has been ignored; this effect will make the track resolution better than predicted from the individual hit resolution.

Multiple Scattering Effects

Momentum resolution for very high momentum tracks is limited by position resolution, but, for most tracks in the STAR TPC, it is dominated by multiple scattering in the gas, especially for P10. The Fig. 15 scatterplots display rms transverse scattering versus crossing angle at the center and ends of the outer-most pad rows for p, $K^\pm$ and $\pi^\pm$. The lines show the hit resolution obtained with the best of the tested reconstruction algorithms at each angle. From this, we do not expect TPC position resolution to play a major role in momentum resolution below several GeV/c, though a full-blown Monte Carlo is needed for any serious study of the momentum resolution; this is beyond the scope of the current study.

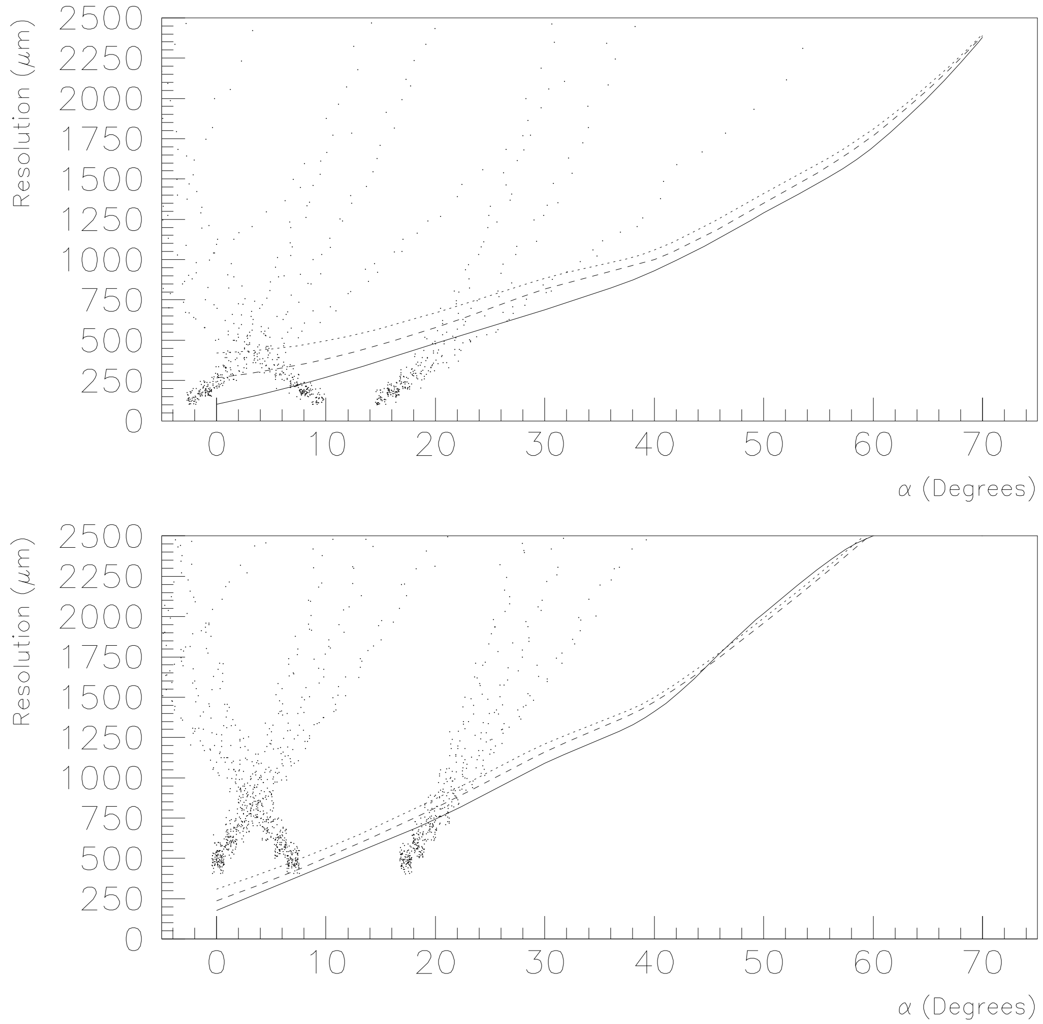

Figure 16: Scatterplots showing transverse scattering (rms) after the innermost TPC row, and crossing angle at the pad row center and ends for p, $K^{\pm}$ and $\pi^{\pm}$ travelling transverse to the beamline. Momenta were distributed uniformly up to 2 GeV/c. The "best" hit resolution is shown for $\sigma_{\rm dif} = 0$ (solid line), $\sigma_{\rm dif} = 0.185$ cm (dashed line) and $\sigma_{\rm dif} = 0.262$ cm (dotted line). The figures are for a) pad row 13 (last inner row) and b) pad row 45 (last outer row). Tracks were propagated from the TPC center without energy loss or scattering.

To semi-quantitatively estimate the momentum P_{equal} at which multiple scattering and resolution contribute equally to momentum resolution for the TPC alone, the Particle Data Booklet formulae[19] can be used:

$$\delta k_{\mathrm{res}} = \frac{\epsilon}{L'^2}\sqrt{\frac{720}{N+4}} \approx \frac{0.0400\mathrm{cm}}{(130\mathrm{cm})^2}\sqrt{\frac{720}{45+4}} \approx 9.07\times 10^{-6} \text{ and}$$

$$\delta k_{\mathrm{ms}} = \frac{(0.016\mathrm{GeV/c})z}{Lp\beta\sin^2\theta}\sqrt{\frac{L}{X_0}} \approx \frac{(0.016\mathrm{GeV/c})}{(150\mathrm{cm})P_{\mathrm{equal}}\sin^2 60^\circ}\sqrt{\frac{150\mathrm{cm}}{12,960\mathrm{cm}}} = \frac{1.53\times 10^{-5}}{P_{\mathrm{equal}}} \ .$$

Symbols are analogous to those defined in the reference. From this, P_{equal} =1.7 GeV/c.

TPC Anode Voltages

As discussed before, simulations for this note used effective gas gains of 1350 (inner) and 615 (outer). Since these gains seem reasonable, the corresponding operating voltages are of interest. Scaling the empirical formula for gas gain in P10[20] by 0.90 to compensate for the shaping time difference, one obtains

$$G(E_g) = 0.000760\exp\left(0.0757\frac{\mathrm{cm}}{\mathrm{kV}}\cdot E_g\right) \ ,$$

where E_g is the electric field at the anode wire surface. $E_g = CV/2\pi\epsilon_0 r$ for an anode voltage V, capacitance/length C and radius r, so

$$G(V) = 0.000760\exp\left(0.0757\frac{\mathrm{cm}}{\mathrm{kV}}\cdot\frac{V}{r}\frac{C}{2\pi\epsilon_0}\right) \ .$$

Substituting the wire radius of 0.0010 cm and Garfield estimates that $C_{\mathrm{inner}}/2\pi\epsilon_0 = 0.172$ and $C_{\mathrm{outer}}/2\pi\epsilon_0 = 0.136$,

$$G_{\mathrm{inner}}(V) = 0.000760\exp\left(\frac{13.05}{\mathrm{kV}}V_{\mathrm{inner}}\right) \text{ and}$$

$$G_{\mathrm{outer}}(V) = 0.000760\exp\left(\frac{10.26}{\mathrm{kV}}V_{\mathrm{outer}}\right) \ ;$$

or

$$V_{\mathrm{inner}} = \ln\left(\frac{G_{\mathrm{inner}}}{0.000760}\right)\frac{\mathrm{kV}}{13.05} = 1100 \text{ V and}$$

$$V_{\mathrm{outer}} = \ln\left(\frac{G_{\mathrm{outer}}}{0.000760}\right)\frac{\mathrm{kV}}{10.26} = 1330 \text{ V} \ .$$

[19] Particle Data Booklet (1994), Formulae 12.18 and 12.19.

[20] Draft STAR Note, W. Betts *et al.*

Crossing Angle Estimation

For the first-pass tracking, one has only local cluster information from which to estimate the crossing angle and select the appropriate algorithm. By way of illustration, one would like to use the weighted mean algorithm for crossing angles above 22° (inner) and 30° (outer), but doesn't know the crossing angle accurately. The STAR TPC clusterfinder estimates the crossing angle[21] with a typical accuracy of 15° (with long, non-Gaussian tails) from the cluster width; this is good enough to select the correct algorithm at large crossing angles, but is marginal for small angles.

One can hope for more accuracy by exploiting the more-or-less known diffusion width for a given pixel. A higher accuracy should also be possible in the transition region where the crossing angle is beginning to distort the charge distribution, causing the three-point algorithm to lose accuracy. Figures 17 and 18 display fitted, uncorrected "Gaussian" widths for such tracks at two crossing angles, separated by 20°. The width distributions are reasonably distinct in the outer subsector, but nearly merge for long drift distances in the inner subsector.

The poor separation in the latter case is not entirely due to the information lost by diffusion; as we have seen, a significant part of the charge is spread beyond the central three pads. Figures 19 and 20 display the results with five pads; the distributions for the worst case are improved, but not cleanly separated. Additional improvement is undoubtedly possible, but this gives an idea of what can be done trivially.

In short, hits for which the weighted mean algorithm is preferred can be reasonably well determined using only local cluster information, except for drift distances beyond a meter in the inner subsector. Here, the weighted mean resolution is not too much worse than the alternatives, and relatively little is lost by biasing the choice in its favor.

Conclusions

Refinement of the STAR TPC position algorithm can improve the TPC hit resolution in both first- and second-pass tracking. From simulations that included ionization statistics and other corrections, the CDR values for TPC base resolution can probably be achieved at $G_{\text{inner}} = 1350$ and $G_{\text{outer}} = 615$, even without global tracking information; for second-pass tracking, with known crossing angles, resolution should surpass the CDR values at these gains. Anode wire voltages of $V_{\text{inner}} = 1100$ V and $G_{\text{outer}} = 1330$ V are required. On the other hand, the diffusion and crossing angle effects are found to be larger than the CDR estimates (though the three-pad algorithm used in the STAR simulation chain would make the crossing angle effect even larger in many cases). Figures 13, 14 show estimates of the improvement possible over the simple three-pad algorithm.

[21] STAR Note SN0238, Mike Lisa, Fig. 29, (1996).

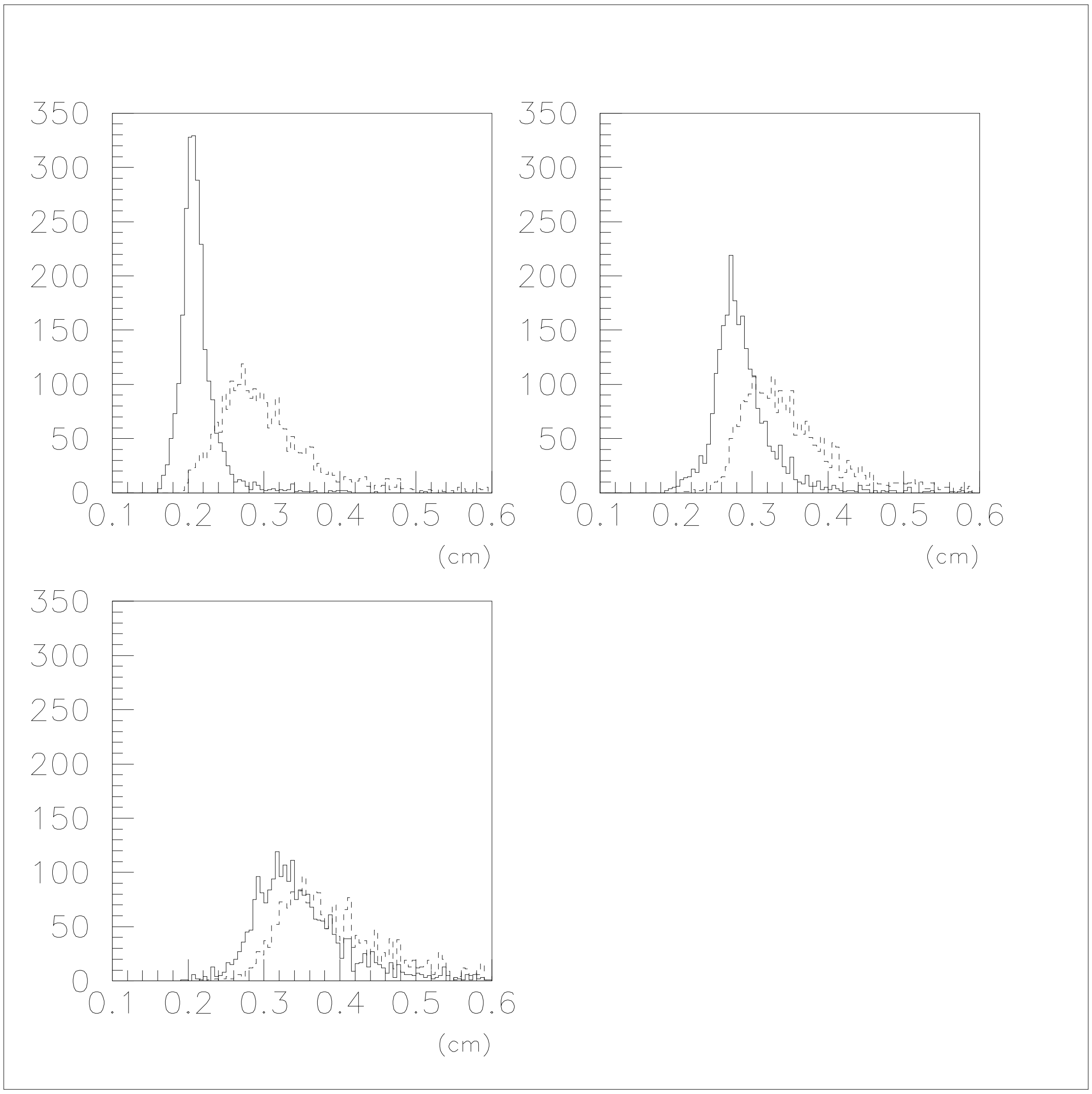

Figure 17: Uncorrected widths fitted with the three-pad algorithm for simulated, minimum-ionizing hits in the inner subsector; crossing angles were α=10° (solid lines) and 30° (dashed lines). The plots are for a) $\sigma_{\text{dif}} = 0$, b) $\sigma_{\text{dif}} = 0.185$ cm and c) $\sigma_{\text{dif}} = 0.262$ cm.

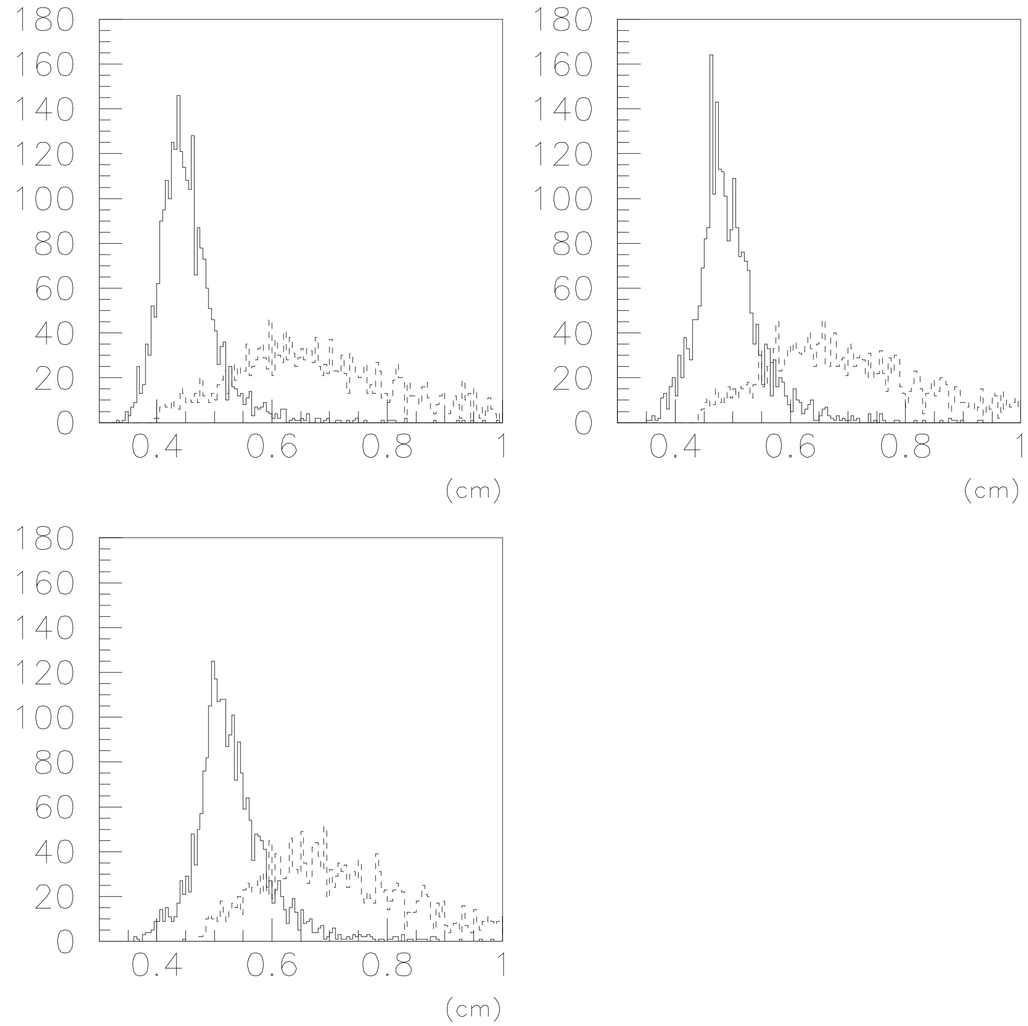

Figure 18: Uncorrected widths fitted with the three-pad algorithm for simulated, minimum-ionizing hits in the outer subsector; crossing angles were α=20° (solid lines) and 40° (dashed lines). The plots are for a) $\sigma_{\text{dif}} = 0$, b) $\sigma_{\text{dif}} = 0.185$ cm and c) $\sigma_{\text{dif}} = 0.262$ cm.

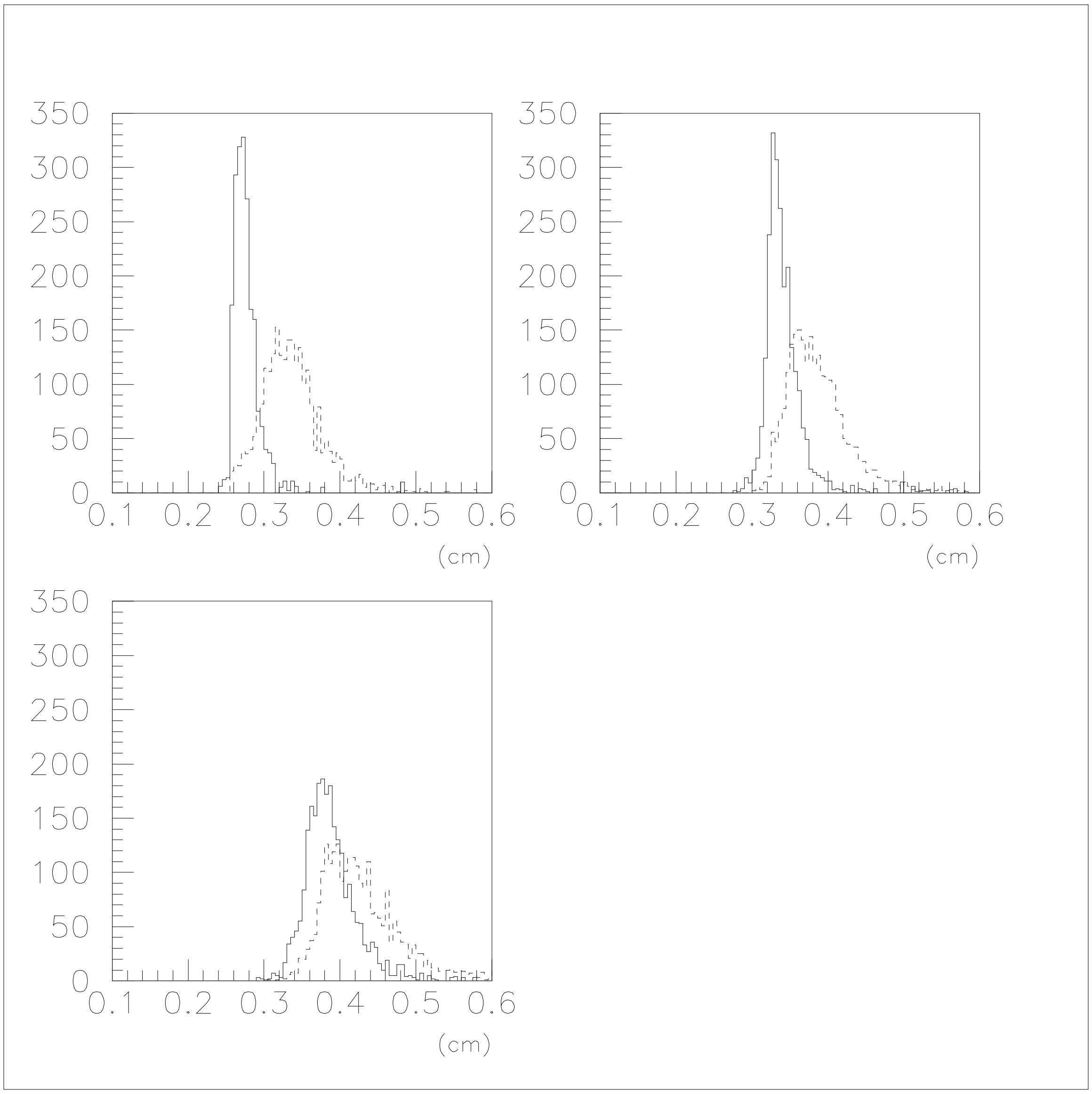

Figure 19: Uncorrected widths fitted with a five-pad algorithm for simulated, minimum-ionizing hits in the inner subsector; crossing angles were α=10° (solid lines) and 30° (dashed lines). The plots are for a) $\sigma_{\rm dif} = 0$, b) $\sigma_{\rm dif} = 0.185$ cm and c) $\sigma_{\rm dif} = 0.262$ cm.

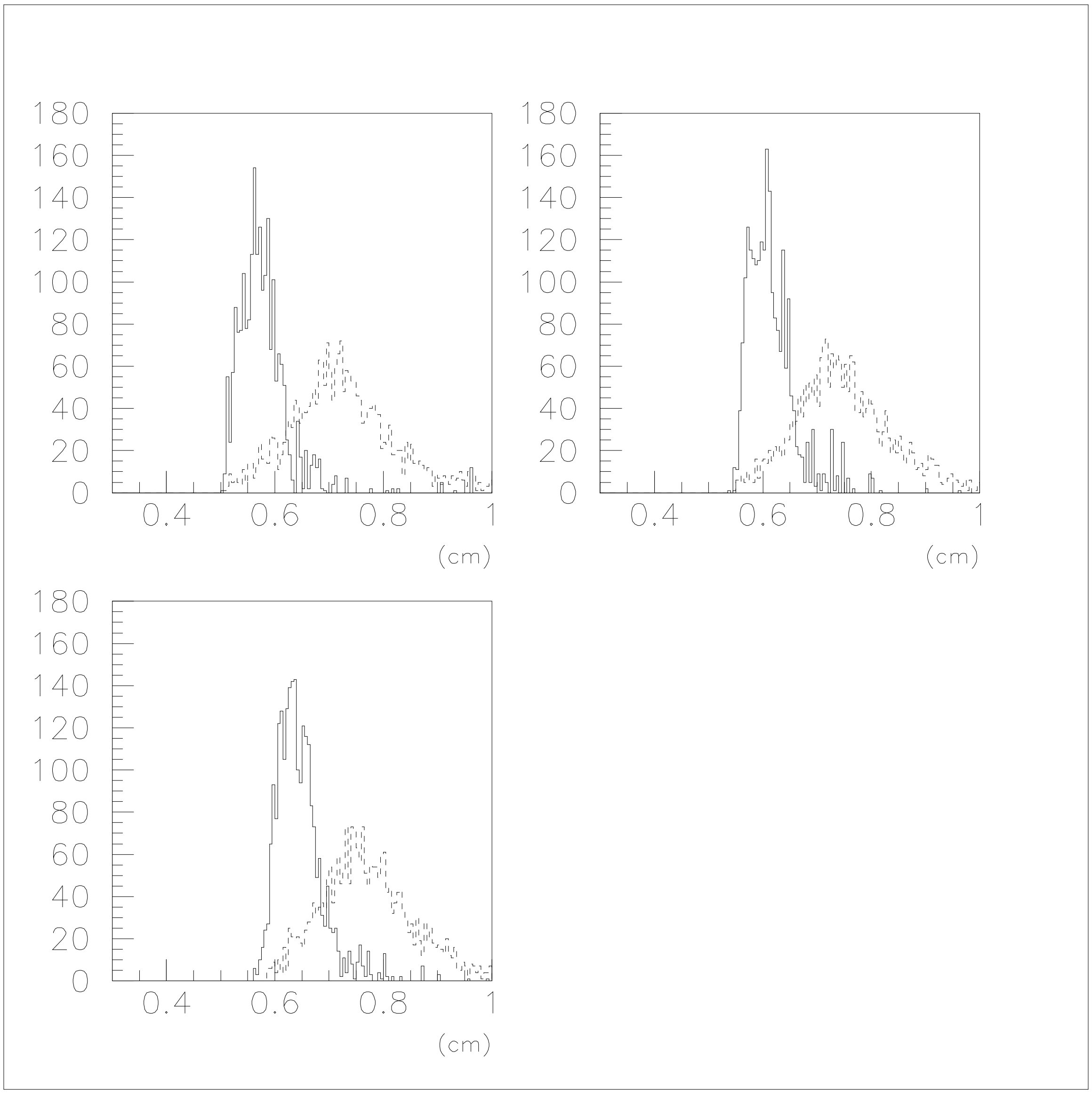

Figure 20: Uncorrected widths fitted with a five-pad algorithm for simulated, minimum-ionizing hits in the outer subsector; crossing angles were α=20° (solid lines) and 40° (dashed lines). The plots are for a) $\sigma_{\rm dif} = 0$, b) $\sigma_{\rm dif} = 0.185$ cm and c) $\sigma_{\rm dif} = 0.262$ cm.